

BABEȘ-BOLYAI UNIVERSITY  
Faculty of Physics



***Cristian Leoștean***

PhD. Thesis summary

**Correlation between nanostructure and  
physical and chemical properties  
of magnetic nanoparticles**

***Scientific supervisor***

***Prof. Dr. Marin Coldea***

2011



## *Thesis content*

<b>I. Introduction</b> .....	<b>1</b>
<b>II. Magnetic properties of the nanoparticles</b> .....	<b>6</b>
2.1. The size effect on the magnetic properties of the nanoparticles.....	6
2.2. Superparamagnetism.....	8
2.3. Magnetic anisotropy of the nanoparticles.....	13
2.4 Magnetization reversal via Stoner-Wohlfart model.....	16
2.5. Magnetic interparticle interactions.....	21
2.6. Magnetic hysteresis curves of the nanoparticles.....	23
2.7. The temperature dependences of the magnetization in zero field cooling and field cooling regimes ZFC-FC.....	27
<b>III. Synthesis conditions of the nanocomposites</b>	
<b>Fe<sub>3</sub>O<sub>4</sub>@PPy, Fe@Au, La<sub>0.67</sub>Sr<sub>0.33</sub>MnO<sub>3</sub>@Au and La<sub>0.67</sub>Sr<sub>0.33</sub>MnO<sub>3</sub>@PPy</b> .....	<b>30</b>
3.1. Core-shell nanoparticles synthesis methods.....	30
3.1.1. Inverse micelles synthesis method.....	30
3.1.2. Sol-gel synthesis method.....	31
3.1.3. Covering the magnetic nanoparticles with polypyrrol (PPy).....	32
3.2. Fe <sub>3</sub> O <sub>4</sub> @PPy nanocomposites preparation.....	33
3.3. Fe@Au nanocomposites preparation.....	34
3.4. La <sub>0.67</sub> Sr <sub>0.33</sub> MnO <sub>3</sub> @Au nanocomposites preparation.....	35
3.5. La <sub>0.67</sub> Sr <sub>0.33</sub> MnO <sub>3</sub> @PPy nanocomposites preparation.....	37
<b>IV. Morphological and structural characterization of the nanocomposites</b>	
<b>Fe<sub>3</sub>O<sub>4</sub>@PPy, Fe@Au, La<sub>0.67</sub>Sr<sub>0.33</sub>MnO<sub>3</sub>@Au and La<sub>0.67</sub>Sr<sub>0.33</sub>MnO<sub>3</sub>@PPy</b> .....	<b>38</b>
4.1. Electronic microscopy.....	38
4.2. X-Ray diffraction.....	44
4.3. Experimental results.....	48
4.3.1. Morphology of Fe <sub>3</sub> O <sub>4</sub> @PPy nanocomposites.....	48
4.3.2 Morphology and structure of Fe@Au nanocomposites.....	53
4.3.3. Morphology and structure of La <sub>0.67</sub> Sr <sub>0.33</sub> MnO <sub>3</sub> @Au nanocomposites .....	58
4.3.4. Morphology of La <sub>0.67</sub> Sr <sub>0.33</sub> MnO <sub>3</sub> @PPy nanocomposites.....	65
<b>V. Magnetic and spectroscopic properties of the nanocomposites</b>	
<b>Fe<sub>3</sub>O<sub>4</sub>@PPy, Fe@Au, La<sub>0.67</sub>Sr<sub>0.33</sub>MnO<sub>3</sub>@Au and La<sub>0.67</sub>Sr<sub>0.33</sub>MnO<sub>3</sub>@PPy</b> .....	<b>67</b>
5.1. Vibrating sample magnetometer.....	67
5.2. SQUID magnetometer .....	68
5.3. X-Ray photoelectron spectroscopy.....	72
5.4. Experimental results.....	82
5.4.1. Magnetization of Fe <sub>3</sub> O <sub>4</sub> @PPy nanocomposites.....	82
5.4.2. XPS spectra and magnetization of Fe@Au nanocomposites.....	92
5.4.3. Magnetization of La <sub>0.67</sub> Sr <sub>0.33</sub> MnO <sub>3</sub> @Au nanocomposites.....	101
5.4.4. XPS and XANES spectra and magnetization of La <sub>0.67</sub> Sr <sub>0.33</sub> MnO <sub>3</sub> @PPy nanocomposites.....	106

<b>VI. Conclusions</b> .....	<b>112</b>
<b>References</b> .....	<b>117</b>
<b>List of published papers</b> .....	<b>124</b>
<b>List of communications</b> .....	<b>125</b>

**Keywords:** Nanoparticles, Core–shell superparamagnetic particles, Hybrid materials, polypyrrol

## Chapter I. Introduction

There is growing interest in studying materials at nanometric scale both from fundamental point of view and new technological applications [1,2].

The interesting and sometimes unexpected properties of the nanoparticles are attributed mainly to the surface atoms. In the case of the magnetic nanoparticles by reducing the size, a transition from polydomain to monodomain occurs [3]. In these systems if the thermal energy is strong enough, a superparamagnetic behavior can be observed [4].

An interesting system of magnetic nanoparticles is core-shell nanoparticles. Essential for the applications of these systems is the control of their magnetic properties. In this purpose a solution is to cover the magnetic core with a layer from another material which can tailor the system properties. The magnetic core can be covered with a non-magnetic layer or antiferromagnetic or ferro/ferri-magnetic.

In this PhD thesis I studied the morphological, structural, magnetic and spectroscopic properties of four nanoparticle systems:  $\text{Fe}_3\text{O}_4@\text{PPy}$ ,  $\text{Fe}@\text{Au}$ ,  $\text{La}_{0.67}\text{Sr}_{0.33}\text{MnO}_3@\text{Au}$  and  $\text{La}_{0.67}\text{Sr}_{0.33}\text{MnO}_3@\text{PPy}$ .

The aim of the thesis was to obtain core-shell magnetic nanoparticles, to study their morphological, structural, magnetic and spectroscopic properties according to the synthesis conditions and to explain the physical phenomena that take place at the core and shell, and the saturation magnetization dependence on the synthesis method.

The scientific contribution of the thesis is the use of new synthesis conditions, which reflects in new properties, to reach the desired demands of various applications and to improve performance.

Core-shell magnetic nanoparticle structures with a gold shell are recently reported that improve chemical stability by protecting the magnetic core from oxidation and corrosion, and show a good biocompatibility and affinity by amino/thiol terminal groups.

The hybrid magnetic nanoparticle structures with polypyrrol attracted special attention from the fundamental and applicative point of view, due to their special unique properties, that are hard to obtain only in each of the component materials. The hybrid structures magnetic nanoparticle – polymer allow the functionalization and control of the magnetic nanoparticle properties by the structure and composition of the polymer [15-18]. The special properties of the polymers such as: structural stability, elasticity, corrosion resistance, mechanic resistance, the polymers easy synthesis, can be used with the magnetic and optic properties of the nanoparticles to obtain new multifunctional materials.

## Chapter II. Magnetic properties of the nanoparticles

Chapter II consists of an analysis of the magnetic properties of the magnetic nanoparticles, the size effect on the magnetic properties, superparamagnetic behavior, magnetic anisotropy for nanoparticles, magnetization reversal via Stoner-Wohlfart model, magnetic interparticle interactions, the magnetic hysteresis curve and temperature dependence of the magnetization in zero field cooling and field cooling regimes ZFC-FC.

In order to establish that a sample is superparamagnetic at least two conditions must be accomplished:

- (i) in the thermodynamic limit and finite time scale, the magnetization *vs.* applied magnetic field show no hysteresis (very small coercitive field)
- (ii) with the exception of interparticle interactions, the magnetization of an isotropic sample must be temperature dependent in a way that the  $M/M_s$  *vs.*  $H/T$  curves taken at different temperatures must approximately superimpose.

## Chapter III. Synthesis conditions of the nanocomposites

$\text{Fe}_3\text{O}_4@PPy$ ,  $\text{Fe}@Au$ ,  $\text{La}_{0.67}\text{Sr}_{0.33}\text{MnO}_3@Au$  and  $\text{La}_{0.67}\text{Sr}_{0.33}\text{MnO}_3@PPy$

In chapter III the synthesis methods and the preparation conditions of the four nanoparticle systems ( $\text{Fe}_3\text{O}_4@PPy$ ,  $\text{Fe}@Au$ ,  $\text{La}_{0.67}\text{Sr}_{0.33}\text{MnO}_3@Au$  and  $\text{La}_{0.67}\text{Sr}_{0.33}\text{MnO}_3@PPy$ ) are described

The magnetite nanoparticles were synthesized through coprecipitation of  $\text{Fe}^{3+}$ ,  $\text{Fe}^{2+}$  ions in solution, with  $\text{NH}_4\text{OH}$  in excess. Combinations of surfactants with different chain lengths: myristic acid (MA), lauric acid (LA) and dodecyl-benzene-sulphonic acid (DBS) were used, such as LA + DBS, MA + DBS and DBS + DBS. The magnetic nanocomposites were prepared by oxidative polymerization of pyrrole in aqueous solution using ammonium peroxodisulfate as an oxidant in the water based magnetic nanofluid. Details of the synthesis condition are presented in Table 3.1.

*Table 3.1 Elemental analysis of PPy- $\text{Fe}_3\text{O}_4$  nanocomposites determined by ICP-AES*

<b>Sample</b>	<b>magnetic nanofluid</b>	<b>C (%)</b>	<b>H (%)</b>	<b>N (%)</b>	<b>S (%)</b>	<b>Fe (%)</b>	<b><math>\text{Fe}_3\text{O}_4</math> (%)</b>
PPy-F1	$\text{Fe}_3\text{O}_4/$ MA+DBS	22.63	3.07	1.79	1.07	44.50	61.45
PPy-F2	$\text{Fe}_3\text{O}_4/$ LA+DBS	21.32	3.08	1.11	0.88	46.20	63.79
PPy-F3	$\text{Fe}_3\text{O}_4/$ DBS+DBS	16.97	1.96	2.32	1.33	48.40	66.83
PPy-F4*	$\text{Fe}_3\text{O}_4/$ DBS+DBS	13	1.82	1.32	0.88	54.80	75.67

\* Sample obtained by pyrrole polymerization at  $0^\circ\text{C}$ .

The iron–gold core–shell nanoparticles (Fe@Au) were prepared by reverse micelle method using cetyltrimethylammonium bromide (CTAB) as surfactant and 1-butanol as cosurfactant. Details of the synthesis condition are presented in Table 3.2.

*Table 3.2. Fe@Au core-shell nanoparticles synthesis conditions*

Sample	Molar ratio		
	surfactant : HAuCl <sub>4</sub>	surfactant : FeSO <sub>4</sub>	FeSO <sub>4</sub> : HAuCl <sub>4</sub>
FA1	10.4	14	1.5
FA2	2.1	14	1.8
FA3	8.2	14	7.2

The La<sub>0.67</sub>Sr<sub>0.33</sub>MnO<sub>3</sub> manganite was prepared by a sol–gel procedure using diethylenetriaminepentaacetic acid as the gelificant agent [61-64]. Coating of the pre-synthesized manganites with gold shells was performed by the seeding method. Details of the synthesis condition are presented in Table 3.3.

*Table 3.3 The synthesis conditions for the LSA samples and samples composition (wt%)*

Sample	Molar ratio Au(OOCCH <sub>3</sub> ) <sub>3</sub> : LSMO	Concentration in synthesis solution (wt%)			Concentration determined by ICP-AES (wt%)			
		Au	Sr	Mn	Au	Sr	Mn	LSMO
		LSA1	5	81.47	2.40	4.58	83.23	1.70
LSA2	2.5	68.59	4.08	7.72	67.08	2.96	5.62	23.0
LSA3	1	31.48	8.90	16.84	33.10	6.83	13.19	54.0

The magnetic nanocomposites based on polypyrrole La<sub>0.67</sub>Sr<sub>0.33</sub>MnO<sub>3</sub>@PPy were prepared by oxidative polymerization of pyrrole (Py) in aqueous solution using ammonium peroxodisulfate (APS) as an oxidant in the water based manganite. Details of the synthesis condition are presented in Table 3.4.

*Table 3.4. Synthesis condition of the LSMO@PPy nanocomposites*

Sample	Py/LSMO molar ratio	oleic acid surfactant
LSMO	-	da
#1	0.66	da
#1'	0.66	nu
#2	3.33	da
#2'	3.33	nu
#3	6.25	da
#4	10	da

## Chapter IV. Morphological and structural characterization of the nanocomposites

$\text{Fe}_3\text{O}_4@\text{PPy}$ ,  $\text{Fe}@\text{Au}$ ,  $\text{La}_{0.67}\text{Sr}_{0.33}\text{MnO}_3@\text{Au}$  and  $\text{La}_{0.67}\text{Sr}_{0.33}\text{MnO}_3@\text{PPy}$

In chapter IV the experimental techniques for morphological and structural characterization are described. The experimental results include the study of the nanoparticles diameter distributions, and the crystal structure is investigated by X-Ray diffraction.

### 4.3. Experimental results

#### 4.3.1 Morphology of $\text{Fe}_3\text{O}_4@\text{PPy}$ nanocomposites [67-69]

Different size distributions were obtained for the  $\text{Fe}_3\text{O}_4$  nanoparticles depending on the surfactant nature. These differences can be evidenced by plotting the  $Nf(V)$  product as a function of  $V$ , as shown in Fig. 4.7 (a) and (b) where  $V$  represents the volume of nanoparticle and  $f(V)$  is the lognormal distribution expressed as a function of  $V$ . The normalized distribution of diameters is well described by a *lognormal* distribution function: [78]:

$$f(D) = \frac{1}{D\sigma\sqrt{2\pi}} \exp\left[-\frac{1}{2}\left(\frac{\ln^2 D/D_0}{\sigma^2}\right)\right] \quad (4.11)$$

here  $D$  is the diameter,  $D_0$  is the mean diameter and  $\sigma$  is the standard deviation.

One can see from Fig. 4.7(a) that the nanoparticles stabilized with MA+DBS or LA+DBS have a single peak narrow distribution while the distribution obtained for the DBS+DBS ferrofluid has two maxima which likely result from the superposition of two different distributions. The mean diameters obtained by the best fit of the distributions in Fig. 4.7 are shown in Table 4.1.

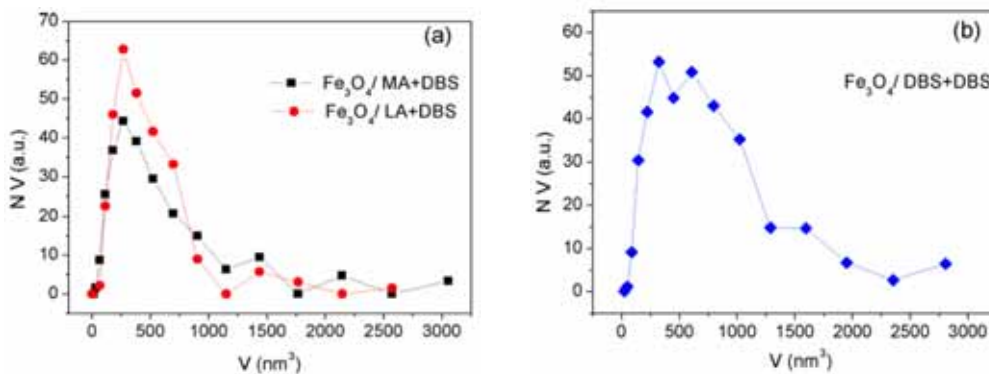


Fig. 4.7  $N(V)$  distributions of the volumes  $V$  of nanoparticles from ferrofluids  
(a)  $\text{Fe}_3\text{O}_4$  stabilized with MA+DBS and LA+DBS, (b)  $\text{Fe}_3\text{O}_4$  stabilized with DBS+DBS

HRTEM images of the magnetic nanocomposites are given in Fig.4.8 and 4.9. The PPy layer is approximately 1.5 - 3.5 nm thick. The thicker PPy layer is observed for the PPy-F3 sample prepared with the  $\text{Fe}_3\text{O}_4/\text{DBS}+\text{DBS}$  ferrofluid at room temperature

and the thinner one for the sample prepared with the same ferrofluid at 0°C (sample PPy-F4).

*Table 4.1. Nanoparticles mean diameter as obtained by TEM*

	Ferrofluid		
	Fe <sub>3</sub> O <sub>4</sub> / MA+DBS	Fe <sub>3</sub> O <sub>4</sub> / LA+DBS	Fe <sub>3</sub> O <sub>4</sub> / DBS+DBS
D <sub>0</sub> <sup>TEM</sup> (nm)	7.2	7.6	7.9
			11.4
σ <sup>TEM</sup>	0.217	0.193	0.19
			0.179

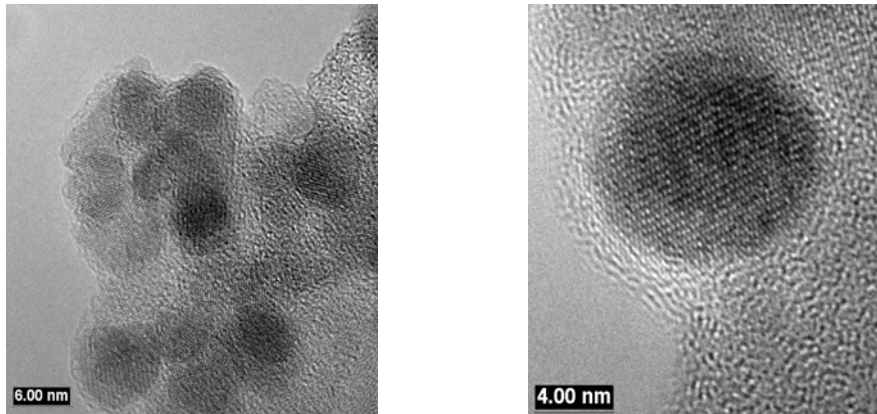


*Fig. 4.9. HRTEM images of the nanocomposite sample PPy-F1 prepared with magnetic nanofluid Fe<sub>3</sub>O<sub>4</sub>/MA+DBS*

### 4.3.2. Morphology and structure of Fe@Au nanocomposites [72]

The diameter distributions of the Fe@Au nanoparticles of the samples FA1, FA2, FA3 are presented in Fig. 4.11. One can see that the nanoparticles size distribution of the FA1 sample is broader. It can be fitted only by using the superposition of two lognormal weighted distributions (the resulted weights are 0.498 and 0.502, respectively). The calculated fit diameters are presented in Table 4.2.

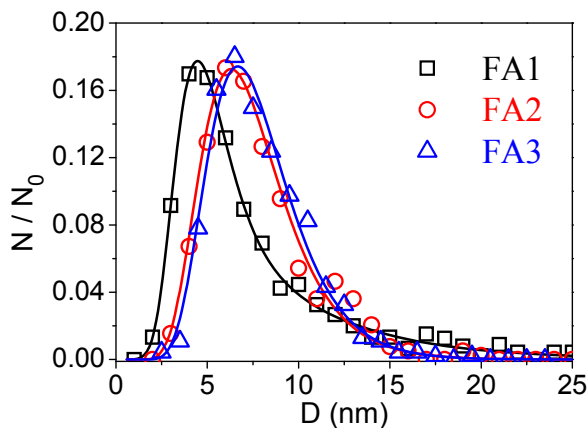


*Fig. 4.11. The diameters distribution of the Fe@Au nanoparticles corresponding to FA1, FA2 and FA3 samples. The continuous lines represent the best fit using the lognormal distribution function*

Table 4.2 Best fit parameters of nanoparticles external mean diameters  $D_0$ , and dispersions  $\sigma$  as resulted from fitting of the diameter distributions by using lognormal distribution

	FA1	FA2	FA3
$D_0$	4.78	7.1	7.4
(nm)	8.57		
$\sigma$	0.32	0.35	0.33
	0.56		

In association of the HRTEM, energy-dispersive X-ray spectroscopy was used to analyze an ensemble of about 50 nanoparticles and separately one single nanoparticle. The spectra are shown in Fig. 4.13 in the case of FA1 sample. One can see that both Au and Fe are present in the recorded spectrum for a single nanoparticle. This fact is in correlation with the XPS data and represents an indication that the core-shell structure is formed.

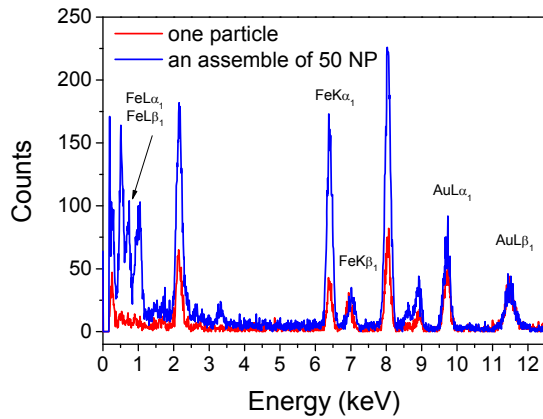


Fig. 4.13. EDX spectra of an ensemble of 50 nanoparticles and separately one single nanoparticle of FA1 sample. One can see that both Au and Fe are present in the spectra

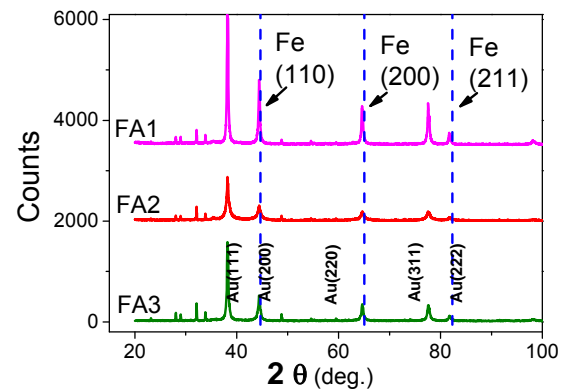


Fig. 4.14. The diffraction patterns of FA1, FA2 and FA3 samples

The XRD patterns of the Fe@Au samples are presented in Fig. 4.14. The mean effective gold nanocrystallite sizes are:

- for the Au shell  $\langle D_{Au} \rangle_1 = 24.5$  nm,  $\langle D_{Au} \rangle_2 = 22.1$  nm,  $\langle D_{Au} \rangle_3 = 24.8$  nm
- for the Fe core  $\langle D_{Fe} \rangle_1 = 14.6$  nm,  $\langle D_{Fe} \rangle_2 = 12.0$  nm,  $\langle D_{Fe} \rangle_3 = 15.1$  nm.

In accordance with core-shell structure, the values determined for Fe core are smaller than the corresponding values determined for the gold shell. On the other hand, for both Au and Fe nanocrystallites, the values calculated from the XRD line profiles are much larger than the values observed from TEM and HRTEM images.

### 4.3.3. Morphology and structure of $\text{La}_{0.67}\text{Sr}_{0.33}\text{MnO}_3@Au$ nanocomposites [73]

For the LSA1 sample (Fig. 4.15) the HRTEM image showing large globular nanoparticles with different shapes suggests that inside some of the globular gold particles different LSMO core nanocrystallites could be found. In the case of LSA2 and LSA3 samples from Fig.4.16, due to the reduction of Au content in the synthesis stage, thinner Au shells will also result and the number of nanoparticles having multiple cores inside a single shell is also significantly reduced. One can also note that the tendency to form regular self-assembled structures in the case of the LSA2 sample.

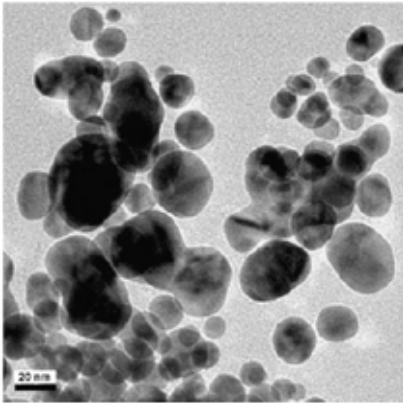


Fig. 4.15. HRTEM image of nanoparticles of LSA1 sample

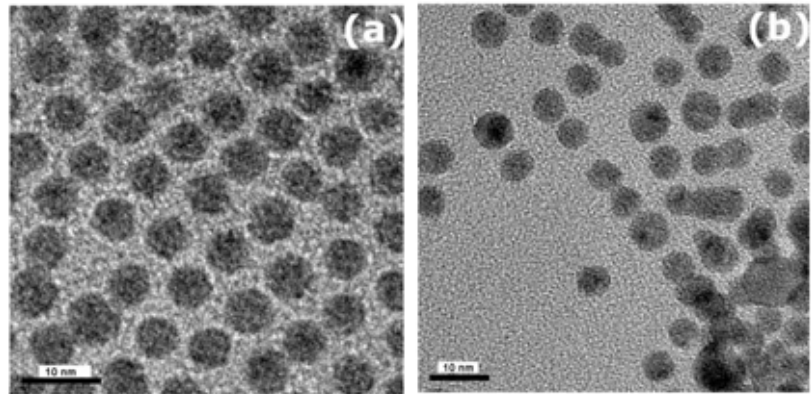


Fig. 4.16. HRTEM images of nanoparticles from samples: (a) LSA2 and (b) LSA3

An ensemble of bare LSMO nanoparticles is presented in the TEM and HRTEM images shown in Fig. 4.17(a) and (b). Here one can observe that alongside well dispersed nanoparticles, some large clusters are also formed.

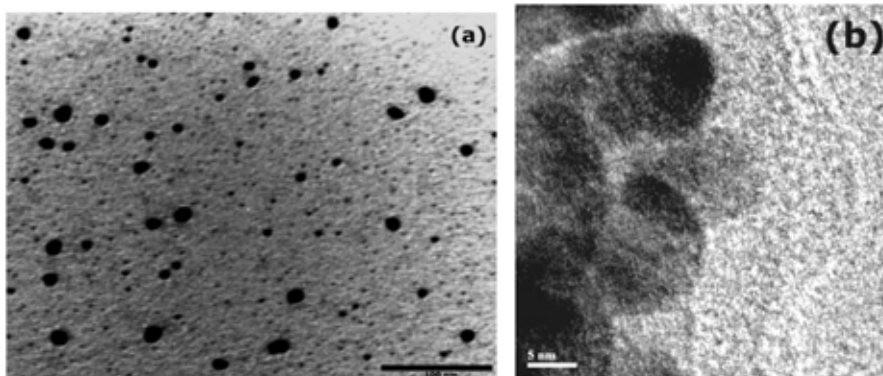


Fig. 4.17 (a) TEM image of an ensemble of nanoparticles from sample LSMO  
(b) HRTEM image of a cluster of nanoparticles from sample LSMO

The diameter distributions of bare LSMO and LSA samples are shown in Fig. 4.18 (a) and (b). The continuous line in Fig. 4.18 (a) represent the best fit using a weighted superposition of two lognormal distributions (the resulted weights are 0.824 and 0.176, respectively). The distribution situated at larger diameters could result in fact from the contributions of nanoparticle aggregates. Aggregation may appear probably due to an insufficient stabilization of the nanoparticles. In Fig. 4.18 one can observe that a narrow size distribution was obtained for the samples LSA2 and LSA3 prepared using Au concentrations lower than 67wt%. It reflects the tendency that is shown in Fig. 4.16.

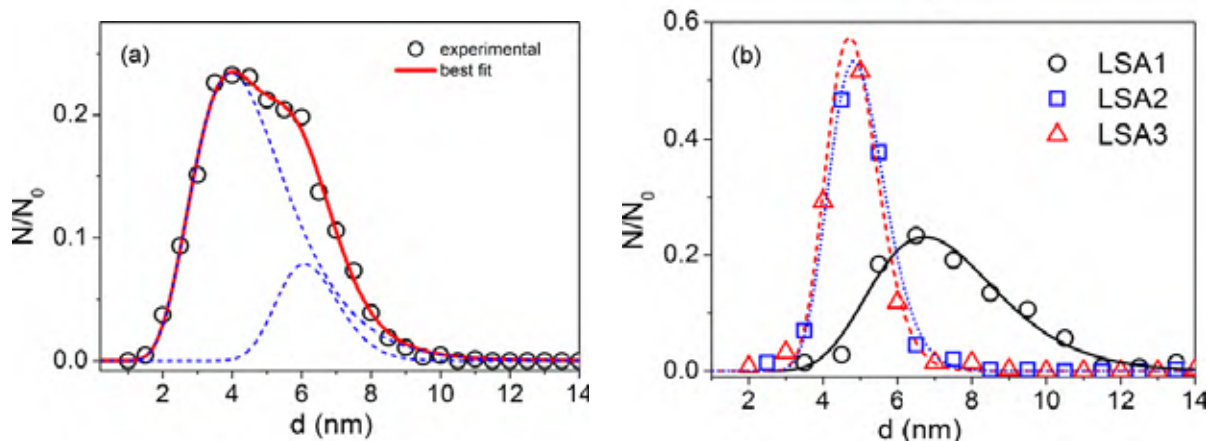


Fig. 4.18. The distributions of nanoparticle diameters determined from TEM images for: (a) bare LSMO nanoparticles and (b) LSA1, LSA2 and LSA3 samples. The continuous lines represent the best fit as obtained by using Eq. (4.11)

The increase of Au concentration in the solution up to 83wt% for sample LSA1 results in a larger size distribution with a peak shifted to higher diameter as compared with the previous case. It suggests that the increase of  $\text{Au}(\text{OOCCH}_3)_3$  in the solution induces a destabilization of the surfactants, coating the manganite nanoparticles, thus changing the interparticles interactions. This mechanism may explain why nanoparticles aggregates are covered by Au, as one can observe from the TEM image of LSA1 sample from Fig. 4.15.

Table 4.3. Best fit parameters of magnetic core-shell LSMO@Au nanoparticles distributions as resulted by using Eq. (4.11). Here  $D_0$  is the mean external diameter, and  $\sigma$  represents the dispersions. The last row displays the estimated values of the mean gold outer shell thickness as resulted by using both  $D_0$  values and the iron/gold wt% ratios from ICP-AES data

	LSMO	LSA1	LSA2	LSA3
$D_0$ (nm)	4.44 6.21	7.15	4.94	0.48
$\sigma$	0.33 0.15	0.23	0.15	0.145
$\delta$ (nm)	-	1.14	0.5	0.15

The best fit parameters of the curves from Fig. 4.18 (a) and (b) are given in Table 4.3. The third row of Table 3 displays the mean values of the gold shell thickness calculated by using the Au/LSMO wt ratios determined by ICP-AES and by using  $\text{La}_{0.67}\text{Sr}_{0.33}\text{MnO}_3$  as stoichiometry. These results show that the thickness of the Au shell covering the magnetic nanoparticles is an important parameter influencing the size distribution of the core-shell nanoparticles. During the synthesis the thin gold shells at the nanoparticles surfaces avoid the aggregates formation due to the reduction of dipolar magnetic interparticles interactions. Therefore a narrow size distribution of small diameter nanoparticles is obtained in this case. Above a critical value of the thickness of the gold shell covering the magnetic nanoparticles, clusters containing gold embedded nanoparticles will appear.

#### 4.3.4. Morphology of $\text{La}_{0.67}\text{Sr}_{0.33}\text{MnO}_3@PPy$ nanocomposites [77]

As an example, HRTEM images of the magnetic nanocomposites are given in the Fig. 4.21 and 4.22. One can observe that nanoparticles are grouped in clusters. All the darker LSMO nanoparticles are surrounded by a clearer layer. This layer is approximately 2 – 3.5 nm thick and the contrast suggests that it should be a polymer (PPy) layer. It is worth noting that the different crystalline atomic planes can be distinguished in some nanoparticles. One can observe that the polymer which surrounds the magnetite nanoparticles seems to be strongly adhesive onto the surface of the nanoparticles resulting in a very intimate connection between the two components. This fact will result into an important interaction between PPy and the surface of the nanoparticles.

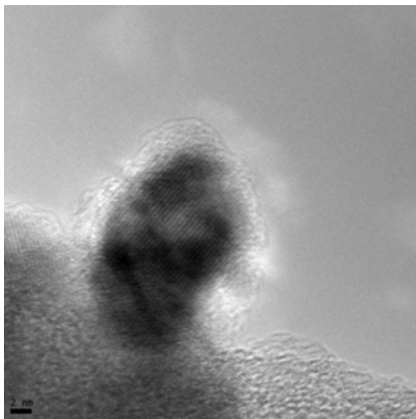


*Fig. 4.21. HRTEM image of a nanocomposite corresponding to sample #3*

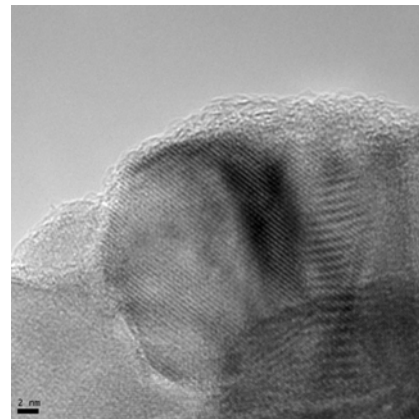


*Fig. 4.22. HRTEM image of a nanocomposite corresponding to sample #4*

A TEM ensemble image is presented in Fig. 4.23. One can observe that the nanoparticles have the tendency to form bundles which in turn are wrapped within a polymeric “cloud”.

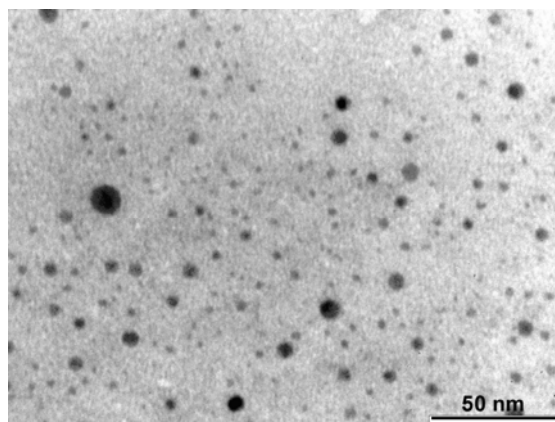


*Fig. 4.23. TEM image of an ensemble corresponding to sample #3*

## Chapter V. Magnetic and spectroscopic properties of the nanocomposites

$\text{Fe}_3\text{O}_4@\text{PPy}$ ,  $\text{Fe}@\text{Au}$ ,  $\text{La}_{0.67}\text{Sr}_{0.33}\text{MnO}_3@\text{Au}$  and  $\text{La}_{0.67}\text{Sr}_{0.33}\text{MnO}_3@\text{PPy}$

In chapter V the experimental techniques used to analyze the magnetic and spectroscopic properties are presented. In the experimental results the hysteresis and ZFC-FC curves are analyzed using the composition determined by XPS or ICP-AES.

### 5.4 Experimental results

#### 5.4.1 Magnetization of $\text{Fe}_3\text{O}_4@\text{PPy}$ nanocomposites [67-69]

The magnetization curves of the PPy nanocomposites, at room temperature, are shown in Fig. 5.14. The data was normalized to the specific magnetite content of each sample. For all samples the magnetic hysteresis curve is typical to a superparamagnetic behavior [82].

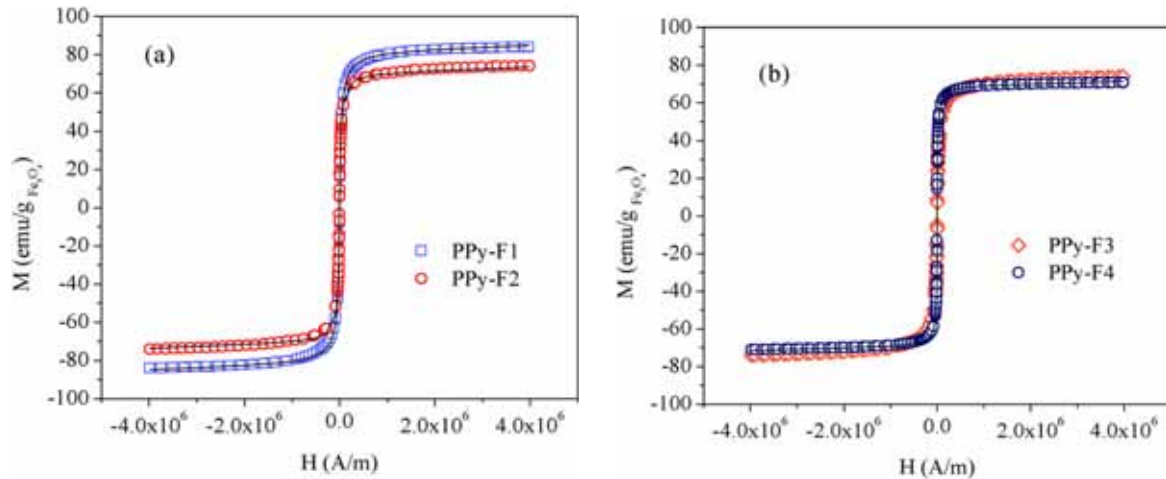


Fig. 5.14. The magnetization curves of the PPy covered nanocomposites, at room temperature. The continuous lines represent the best fit using Eq.(5.12)

As shown in Table 5.1 the combined effect of surfactants and polymer yields to an important increase of the saturation magnetization compared to the values obtained for the nanofluid.

The magnetization of a superparamagnetic system is described by the following equation [92]:

$$M(H, T) = M_s \frac{\int V(D_m) L \left[ \frac{M_s V(D_m) H}{k_B T} \right] f(D_m) dD_m}{\int V(D_m) f(D_m) dD_m} \quad (5.12)$$

here  $V(D_m)$  is volume of the magnetic core of the nanoparticles expressed as a function of diameters  $D_m$  (“magnetic” diameter),  $H$  is the applied external magnetic field and  $f(D_m)$  is the lognormal distribution of diameters given in Eq. (4.11).

The magnetic diameter of a nanoparticle is smaller than its real diameter,  $D_m < D$ . Many authors explained this observation upon the existence of a magnetically disordered or nonmagnetic layer at the nanoparticles surface [85,92-94]. The magnetization curves were fitted using Eq. (5.12). The calculated fit parameters are shown in Table 5.1.

Table 5.1. Characteristic diameters  $D_{0m}$ , dispersions  $\sigma_m$  and saturation magnetizations  $M_s$  calculated for the magnetic cores of the nanoparticles from ferrofluids and for the nanocomposite samples, respectively. The last columns show the values of the effective anisotropy constant,  $K_{eff}$  calculated by combining the fit parameters resulted from  $M(H)$  dependences with ZFC-FC curves

Sample	$D_{0m}$ (nm)	$\sigma_m$	$M_s$ (emu/g $Fe_3O_4$ )	$K_{eff}$ (J/cm <sup>3</sup> )
$Fe_3O_4/MA+DBS$	6.4	0.43	50	$3.1 \times 10^4$
$Fe_3O_4/LA+DBS$	6.4	0.37	49	$3.9 \times 10^4$
$Fe_3O_4/DBS+DBS$	6.6	0.34	65	$4.1 \times 10^4$
	9.46	0.31		$4.3 \times 10^4$
PPy-F1	6.6	0.35	81	$2.6 \times 10^4$
PPy-F2	7.5	0.346	75	$2.6 \times 10^4$
PPy-F3	6.9	0.240	75.7	$6 \times 10^4$
	9.8	0.260		$4 \times 10^4$
PPy-F4	6.4	0.189	71	$3.3 \times 10^4$
	9.2	0.175		$3.5 \times 10^4$

The temperature dependences of the magnetizations of the nanocomposites in zero field cooling (ZFC) and field cooling (FC) regimes are presented in Fig. 5.15. They show a typical superparamagnetic behavior.

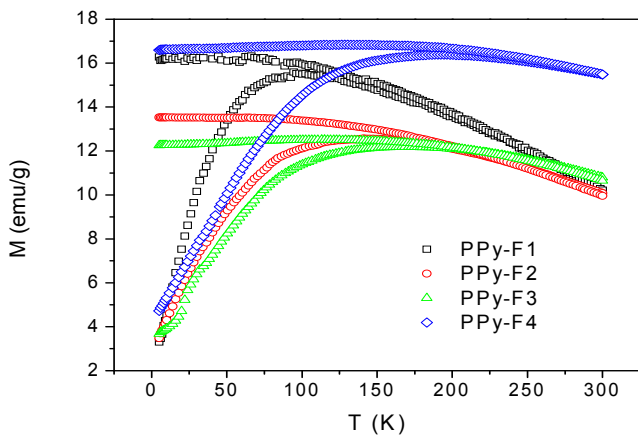


Fig. 5.15. Temperature dependence of the magnetization under zero-field cooling (ZFC) and field cooling (FC) for the magnetic nanocomposites. The applied magnetic field was 100Oe.

In the superparamagnetic regime the difference between FC and ZFC gives the thermo-remnant magnetizations (TRM). The temperature dependence of the TRM is directly correlated with the deblocking process which occurs inside the system of magnetic nanoparticles when the temperature increases in zero applied magnetic field and after a previous FC process. Therefore the TRM is the sum of the moments which are still blocked in the field cooled state. Deblocking occurs when the thermal energy

overcomes the anisotropy energy barrier  $\Delta E_a$ . The energy barrier can be expressed, in a general manner, as [4]:

$$\Delta E_a = KV_m(1 - H/H_c)^2 \quad (5.13)$$

Here  $K$  is the energy density due to axial anisotropy,  $V_m$  is the volume of the magnetically ordered core of the nanoparticles (associated with  $D_m$ ) and  $H_c$  the coercivity field. For the TRM case the following simple equation holds [91]:

$$KV_m(T, H) = k_B T \ln \frac{t_m}{\tau_0} \quad (5.14)$$

where  $\tau_0$  is a microscopic relaxation time (usually in the range of  $10^{-9}$  s),  $k_B$  is the Boltzmann constant and  $t$  the relaxation time necessary to cross the barrier which is usually considered to be equal to the measurement time  $t_m$ .  $t_m$  has typical values ranging between 10 s and 100 s leading to values for  $\ln(t_m/\tau_0)$  between 23 and 27.

It is possible to relate the temperature derivative of the TRM (the  $M_{FC} - M_{ZFC}$  difference) to the energy barriers distribution of the magnetic nanoparticles as shown in Eq (5.15) [95]:

$$\frac{\partial(M_{FC} - M_{ZFC})}{\partial T} = -\frac{M_S^2 k_B H}{3K^2} \frac{\ln^2 t_m / \tau_0}{(1 - H/H_c)^\alpha} V_m(T, 0) f(V_m(T, 0)) \quad (5.15)$$

Fig. 5.16 (a) and (b) display the energy barriers distributions, as deduced from the temperature derivative of the TRM for the magnetic nanoparticles from ferrofluids and for the nanocomposite samples PPy-F1, PPy-F2, PPy-F3 and PPy-F4, respectively. The double peak distribution is evident in the case of  $Fe_3O_4$  nanoparticles stabilized with double layer DBS+DBS in the ferrofluid and also in the nanocomposites prepared using this ferrofluid, samples PPy-F3, PPy-F4.

Using as  $V_m$  the results of the fit of the  $M(H)$  magnetizations, one can extract the axial effective anisotropy constant  $K$  by using Eq (5.14) with  $\ln(t_m/\tau_0) = 25$ . The calculated values of  $K$  are given in Table 5.1 for the magnetite nanoparticles and for the nanocomposite samples. This estimate is valid since the temperatures associated with the peaks of the energy barriers distribution of Fig 5.16 do not depend on the dispersion  $\sigma$  [96].

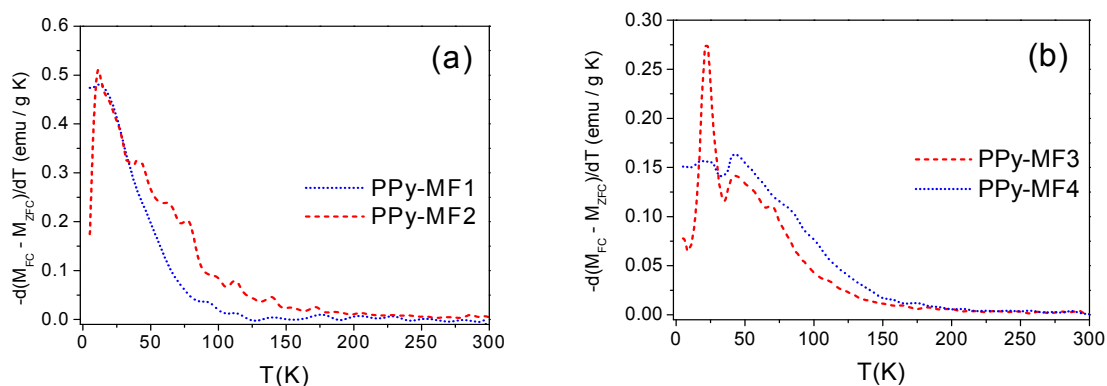


Fig. 5.16. The temperature dependence of the derivative with respect to  $T$  of the  $-M_{TRM}$  magnetizations of (a) PPy nanocomposites prepared with  $Fe_3O_4/MA+DBS$  and  $Fe_3O_4/LA+DBS$  and (b) for PPy nanocomposites prepared with  $Fe_3O_4/DBS+DBS$  samples

The saturation magnetizations  $M_s$  for the three samples of Table 5.1, namely, magnetite nanoparticles covered with different surfactants, is in the range 49–65  $emu/g[Fe_3O_4]$ , in agreement with what is usually reported for magnetite nanoparticles with diameters smaller than 100 nm [83-91]. This value is significantly lower than the bulk value 92  $emu/g$  due to surface spin disorder.

The combined effect of surfactants and PPy leads to an increase in the saturation magnetizations for PPy-F1 and PPy-F4 nanocomposite samples as compared with the corresponding magnetizations of the magnetite nanoparticles. The surface modification of magnetite by polypyrrole coating results in an apparent increase in the magnetic diameter in the case of nanocomposite samples, which could be ascribed to an induced surface spin ordering effect.

In order to investigate the origin of magnetization increase by PPy covering, the infrared absorption spectra was recorded using a JASCO FTIR-6100 spectrophotometer.

Fig. 5.17 compares the FTIR spectrum of a pure PPy sample doped with DBS and the spectra of PPy-F1 and PPy-F3. The FTIR spectra of the nanocomposites contain the characteristic absorption bands of both constituents, namely, oxidized PPy and  $Fe_3O_4$ . The intense absorption band located around  $580\text{ cm}^{-1}$  is characteristic of  $Fe_3O_4$  [97, 98]. The characteristic bands of PPy appear in the  $500\text{--}1700\text{ cm}^{-1}$  region. They are clearly visible in all the spectra. It is well known that the PPy absorption bands are sensitive to the oxidation level and to the conjugation length of the PPy chain [99].

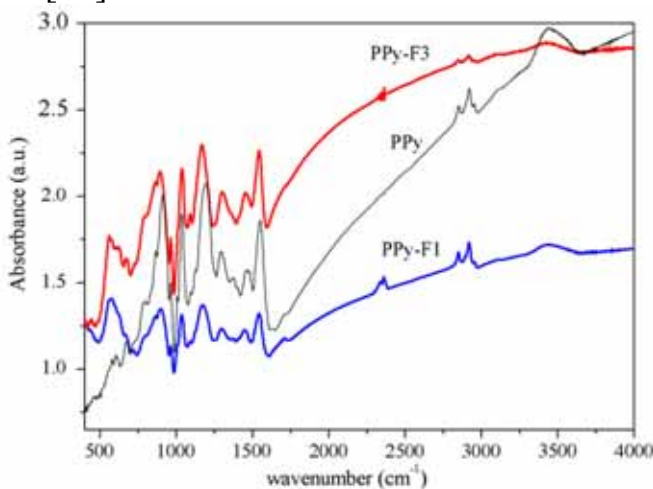


Fig. 5.17 FTIR spectra of PPy doped with DBS and nanocomposites PPy-F1 and PPy-F3

The absorption bands characteristic for pyrrole ring vibrations, located at 914, 1198,  $1465\text{ cm}^{-1}$  in the PPy spectrum, are significantly shifted to lower frequencies in the nanocomposites spectra. This indicates a higher degree of oxidation of PPy in the nanocomposite as compared with conventional PPy [100].

A qualitative explanation of this novel effect of PPy coating on the magnetic properties of magnetite could be given considering the charge transfer process from the conducting polymer to the surface iron ions of magnetite. It involves the laterally delocalized  $\pi$  electrons of the conjugated PPy which could penetrate under the surface of magnetite nanoparticles. Since we are referring to the surface iron ions, this effect is an increase of the surface contribution to the total magnetic moment of the nanocomposites.

### 5.4.2. XPS spectra and magnetization of Fe@Au nanocomposites [72]

The analysis of the Fe 2p core-level XPS lines evidenced that in between the Fe(0) cores and the gold shells there is an additional shell of iron oxides. As it concerns the origin of this inner oxidized shell it seems to result from the oxidation of iron nanoparticles before full covering with gold inside the water inverse micelles dispersed in octane. In accordance to the XPS spectra, the schematic representation of the nanoparticles is presented in Fig. 5.19.

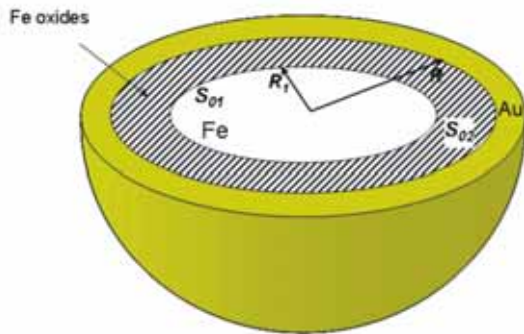


Fig. 5.19. The core-shell structure of a sectioned Fe@Au nanoparticle. The Fe(0) core is surrounded by oxidized iron having an outside gold shell

The oxidized Fe could be seen as a rather disordered mixture of FeO and Fe<sub>2</sub>O<sub>3</sub> [102] since in the XRD patterns did not show any evidence of structurally ordered oxides.

One can consider that, after some long enough etching time, due to the random spatial disposition of nanoparticles, the mean structure of a sectioned nanoparticle could be considered as seen in Fig. 5.19.

Table 5.3. The calculated values of weight and molar contents of the samples as resulted from XPS data

Sample	Fe <sup>(0)</sup>		Fe oxide		Au		CTAB	
	wt%	molar%	wt%	molar%	wt%	molar%	wt%	molar%
FA1	21.83	58.28	57.70	26.92	18.50	13.99	1.97	0.81
FA2	22.22	60.40	58.36	27.72	10.70	8.24	8.72	3.64
FA3	28.47	68.05	59.39	25.40	6.81	4.6	5.33	1.95

The calculated values of weight and molar contents of the samples are shown in Table 5.3.

The magnetization curves vs. the applied magnetic field,  $M = f(H)$  of the Fe@Au samples are presented in Fig. 5.20. The experimental values of the magnetizations, for all the samples, were normalized by dividing to the content of corresponding magnetic material, from Table 5.3. In this way one can compare the magnetic behaviors of samples. As one can see the magnetizations does not show hysteresis loops, having typical superparamagnetic fine particle behaviors.

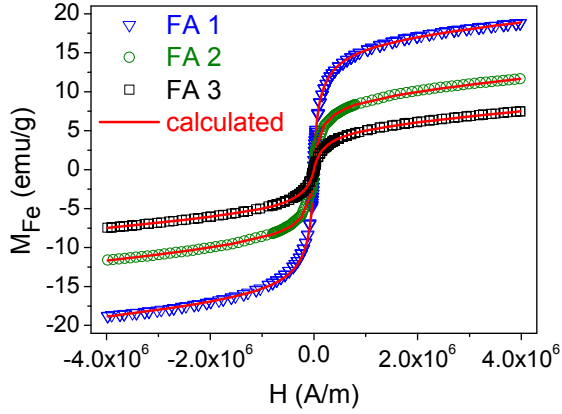


Fig. 5.20. The magnetization curves versus applied magnetic field at room temperature of the Fe@Au samples. The absolute magnetizations are calculated referred to the Fe content of each specific sample. The continuous lines represent the best fits obtained for each sample using Eq. (5.12)

Table 5.4. Characteristic diameters  $D_0^{(m)}$ , dispersions  $\sigma_m$  and saturation magnetizations  $M_S$  calculated for the magnetic cores of the nanoparticles from the FA1-FA3 samples respectively. The last column shows the values of the effective anisotropy constant,  $K_{eff}$  calculated by combining the fit parameters resulted from  $M(H)$  dependences with the analysis of the ZFC-FC curves

Sample	$D_0^{(m)}$ (nm)	$\sigma_m$	$M_S$ (emu/g <sub>(sample)</sub> )	$K_{eff}$ ( $10^5$ J/m <sup>3</sup> )
FA1	2.7	0.26	17.2	9.05
	4.84	0.46		2.23
FA2	4.5	0.49	9.7	2.25
FA3	6.6	0.39	5.5	5.24

The mean “magnetic diameter”  $D_0^{(m)}$  of a ferromagnetic iron core differs from the physical diameter  $D_0$  of the core inside the Au shell. It was shown that the magnetic size of a nanoparticle is smaller than the morphological size. It is due to the formation of a disordered non-magnetic surface layer(s) or, as in our case, an interface layer(s) between the iron core and the oxide shell [85,92-94].

The magnetization data  $M(H)$  were fitted with Eq. (5.12). The calculations were performed following the method presented in Refs [1,67]. In the specific case of FA1 sample, according to Table 5.4, two superposed distributions were used for calculations [67]. The results for the best fit of each sample are shown in Fig. 5.20 by continuous lines. The resulted best fit parameters for the Fe@Au samples are summarized in Table 5.4. As one can see, going from FA1 to FA3, the mean magnetic diameters increase while the saturation magnetizations decrease. This is due to the fact that by increasing the particles mean volumes due to the dispersion of the distributions a larger number of superparamagnetic particles are blocked even at the room temperature.

The temperature dependences of the magnetizations in the ZFC-FC regimes for the Fe@Au samples are shown in Fig. 5.21. One can see a typical superparamagnetic behavior.

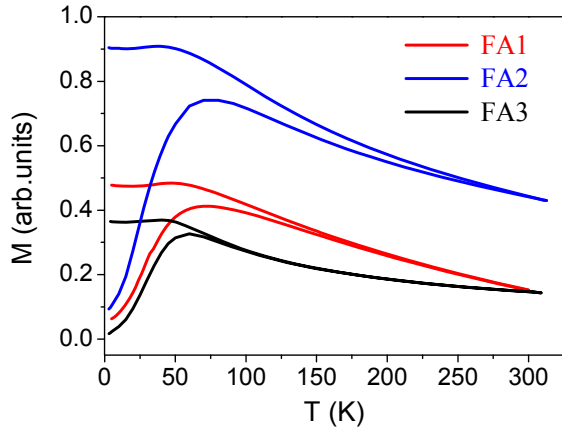


Fig. 5.21 The temperature dependences of the magnetizations in the ZFC-FC regimes for FA1, FA2 and FA3 samples, respectively. The applied magnetic field was 100Oe

The energy barriers distributions, as deduced from the temperature derivative of the TRM for the magnetic core-shell Fe@Au nanoparticles, are shown In Fig. 5.22.

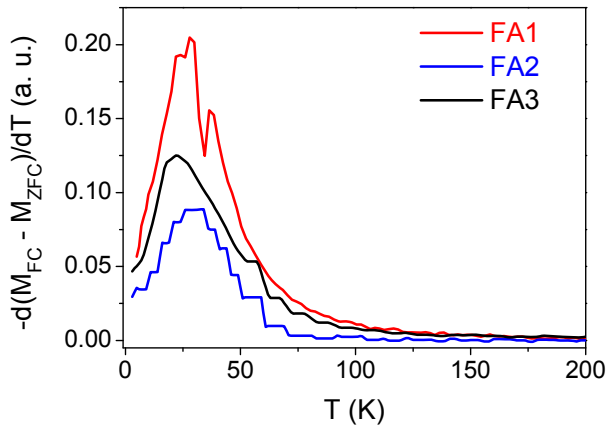


Fig. 5.22. The temperature dependence of the derivative with respect to  $T$  of the  $-M_{TRM}$  magnetizations of core-shell Fe@Au nanoparticles. For the FA1 sample the two maxima are at 26 K and 37 K. For FA2 and FA3 samples the corresponding maxima are at 30 K and 22 K respectively

It should be mentioned that, for the nanometric particles, there is not a linear correspondence between the deblocking temperatures and the volumes of the magnetically ordered cores. In Eq. (5.14) the anisotropy density  $K$  it is not a constant and it should be seen as an effective value  $K_{eff} = K_0 + C K_S$  where  $K_0$  represents the axial volume contribution,  $K_S$  the surface density contribution and  $C$  is a constant specific to a certain nanoparticle [104]. At nanoscale the surface anisotropy  $K_S$  plays an important contribution also being dependent of particle dimensions. The calculated values of  $K_{eff}$  are given in Table 5.4 for the Fe@Au samples by using a mean value of  $\ln(t_m/\tau_0) = 26$ . The calculation was performed following Ref [67]. Usually the equation  $K_{eff} = K_0 + CK_S$  could be expressed as:

$$K_{eff} = K_0 + \frac{6}{D_0^{(m)}} K_S \quad (5.16)$$

In Fig. 5.23 it is presented a plot of  $K_{eff}$  as a function of  $6/D_0^{(m)}$  by using the data from Table 5.4. The size dependence is in accordance with Eq. (5.16) and the slope of the straight line representing the surface contribution is  $K_S = 0.66 \cdot 10^{-3} \text{ J/m}^3$ . For FA1 sample there were considered two sets of values corresponding to the two superposed distributions. One can see that the intersection with  $K_{eff}$  axis is negative. Its absolute value is about  $|K_0| = 5.96 \cdot 10^5 \text{ J/m}^3$  and it is one order of magnitude larger than the usual magnetocrystalline value.

Therefore, it appears that the extrapolated value for  $|K_0|$  does not have any physical significance except its opposed sign relative to  $K_S$ . It seems that combined

shape and stress anisotropy at the gold–iron oxide–iron interfaces are opposed to the crystalline field anisotropy indicating a possible rotation of the easy axis magnetization.

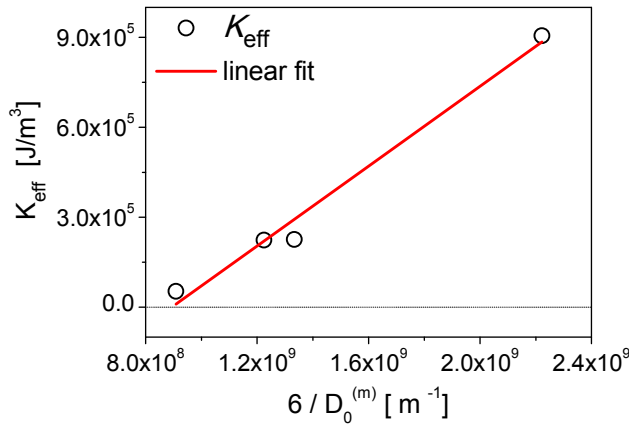


Fig. 5.23. Plot of  $K_{eff}$  as a function of  $6 / D_0^{(m)}$ . According to Eq. (5.16) the slope of the linear fit gives the surface contribution to the effective anisotropy constant

### 5.4.3. Magnetization of $La_{0.67}Sr_{0.33}MnO_3@Au$ nanocomposites [73]

A comparison of the magnetization curves versus the applied magnetic field,  $M=f(H)$  of the bare LSMO nanoparticles as well as of LSMO@Au samples is shown in Fig. 5.24. The experimental values of the magnetizations, for all samples, were normalized by dividing by the content of corresponding magnetic material, as shown in Table 3.3. Typical values of the saturation magnetization for polycrystalline Sr doped manganite, at room temperature, are within 40–65 emu/g range [105,106]. The  $M=f(H)$  curves show no hysteresis loops, indicating a superparamagnetic behavior for the investigated nanoparticles. The continuous lines represent the best fit based on Eq. (5.12).

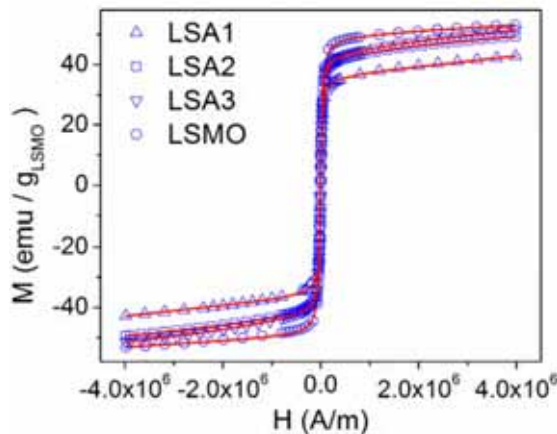


Fig. 5.24. Magnetization versus applied magnetic field dependences at room temperature for LSA1, LSA2 and LSA3 samples together with the bare LSMO sample. The continuous lines represent the best fit of the magnetizations calculated by using Eq. (5.12).

The calculations were performed following the method presented in Ref. [67]. The calculated values are presented in Table 5.5. By comparing the calculated magnetic size distribution parameters  $D_{0m}$  and  $\sigma_m$  with  $D_0$  and  $\sigma$ , previously determined from TEM analysis, one can observe that the calculated diameters are twice larger than the real values determined by using TEM images. The fact represents an indication that, as a result of the dipole–dipole magnetic interactions, the nanoparticles are

gathered in clusters, each particle apparently having a much larger magnetic diameter than the real one.

Table 5.5. Characteristic magnetic diameters  $D_0^m$ , dispersions  $\sigma_m$  and saturation magnetizations  $M_s$  calculated for the magnetic cores of the nanoparticles for the LSMO sample as well as for LSA core-shell samples, respectively.

Sample	$D_0^m$	$\sigma_m$	$M_s$ (emu/g) $\text{La}_{0.67}\text{Sr}_{0.33}\text{MnO}_3$
LSMO	9.9	0.175	49.4
LSA1	9.7	0.31	36.2
LSA2	10.4	0.20	42.5
LSA3	10.1	0.18	44.0

Temperature dependences of the magnetization under ZFC-FC for the bare LSMO nanoparticles and for the LSA1- LSA3 samples are presented in Fig. 5.25, also showing a typical superparamagnetic behavior.

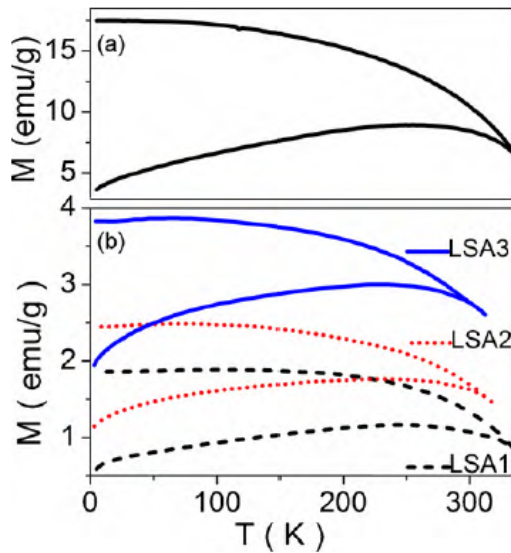


Fig. 5.25. Temperature dependences of the magnetization under zero-field cooling (ZFC) and field cooling (FC) for the (a) bare LSMO nanoparticles and (b) for the LSA1- LSA3 samples. The applied magnetic field was 100Oe

Fig. 5.26 displays the energy barrier distributions, as deduced from the temperature derivative of the TRM for the bare LSMO nanoparticles together with LSA samples. Some two or multiple peak distributions appear in the case of the LSMO sample also appears for the LSA samples. It is less evident in the case of LSA1 nanoparticles where the largest amount of Au is present in the outer shells.

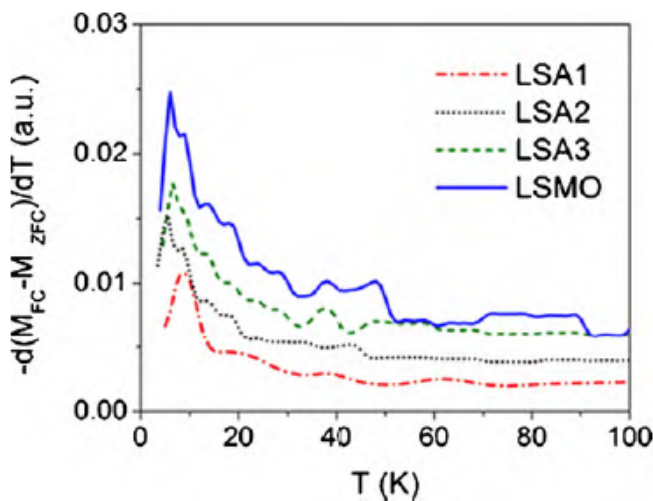


Fig. 5.26. Energy barriers distributions, as deduced from the temperature derivative of the TRM for (a) bare LSMO nanoparticles and (b) LSA1-LSA3 samples

As it was previously mentioned, the disagreement between the calculated “magnetic” diameters and the diameters resulted from TEM images represents an indication that clusters of various dimensions are formed, most probably due to the dipole–dipole magnetic interactions of neighbor nanoparticles. It was shown that the particle interactions influence of height of the energy barrier and affects the blocking temperatures of the nanoparticles [108–110]. Therefore, the total mean height of the energy barrier due to both anisotropy and dipolar interactions could be expressed as [108-110]:

$$\langle \Delta E_{tot} \rangle = KV_0 + \langle n_1 \rangle Y_1 L \left( \frac{Y_1}{k_B T} \right) \quad (5.17)$$

here  $Y_1 = (M_s V_0)^2 \langle (3 \cos^2 \Psi_1 - 1) \rangle / \langle d_1^3 \rangle$ ,  $L$  represents the Langevin function,  $M_s$  is the saturation magnetization,  $V_0$  the mean volume of the ensemble of nanoparticles,  $d_1$  and  $\Psi_1$  designate the positions of the first neighbors,  $\langle d_1 \rangle$  represents the interparticle mean distance and  $\langle n_1 \rangle$  is the mean number of interacting nearest neighbors.

In the weakly interaction limit  $L(x)$  function can be approximated as  $L(x) = x/3$  ( $x < 1$ ) and the mean height of the energy barrier becomes [108]:

$$\langle \Delta E_{tot} \rangle = KV_m + \langle n_1 \rangle \frac{Y_1^2}{3k_B T} \quad (5.18)$$

In the strong interaction limit the Langevin function is given by  $L(x) = 1 - 1/x$  ( $x \geq 2$ ), and Eq.(5.17) becomes

$$\langle \Delta E_{tot} \rangle = KV_m + \langle n_1 \rangle Y_1 - \langle n_1 \rangle k_B T \quad (5.19)$$

The temperature dependence of  $\langle \Delta E_{tot} \rangle$  was made by integrating energy barrier distribution functions over the blocked states (in the upward sense starting from a given  $T$ ), in a similar manner as shown in Eq. (2.31) where the temperature (the blocking temperature) appears in the lower bound of the integral.

$$M_{TRM}(T) = \frac{M_s^2 H}{3k_B} \int_{V_b(T,0)}^{\infty} \frac{f(V)V^2}{T_b(V,H)} dV \quad (2.31)$$

The dipolar interaction acts in order to increase the height of the energy barriers therefore increasing the deblocking temperatures. As compared to the noninteracting case, as the temperature increases, as a consequence of the dipole–dipole interactions, the occurring of the nanoparticles deblocking process is “slowed down” [108]. The dipole–dipole interaction became less important for the already deblocked nanoparticles where the magnetizations are governed by thermal fluctuations. The calculated temperature dependences of  $\langle \Delta E_{tot} \rangle$  for the bare LSMO sample together with gold covered LSA nanoparticle samples are presented in Fig. 5.27. The linearity dependences having negative slopes, as given by Eq. (5.19), indicates that strong dipole–dipole interactions are present between blocked nanoparticles in all the cases. According to Eq. (5.19) the absolute value of the slope is proportional to the mean number of interacting nearest neighbors  $\langle n_1 \rangle$ . Therefore,

weaker interactions (lower  $\langle n_1 \rangle$ ) are present in the case of LSA1 sample which possess a thick gold shell as compared to the LSMO sample.

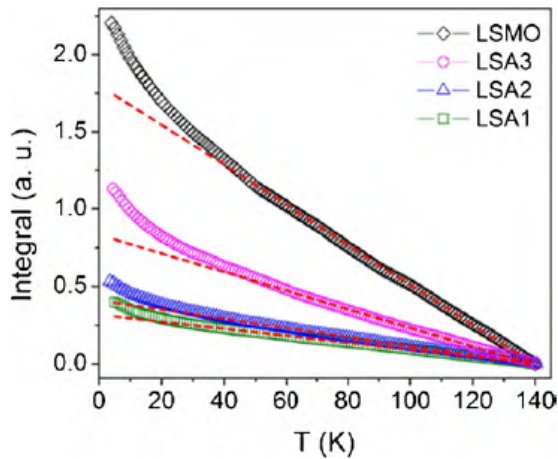


Fig. 5.27. Temperature dependences of mean energy barrier heights for the LSMO sample together with the core-shell LSA1–LSA3 samples. One can observe that higher the gold content (going from LSMO to LSA1) smallest the slope of the main linear part of the graphs and of the number of particles in clusters with dipole–dipole interactions.

#### 5.4.4. XPS and XANES spectra and magnetization of $\text{La}_{0.67}\text{Sr}_{0.33}\text{MnO}_3@PPy$ nanocomposites [77]

The composition of the samples was determined using the XPS technique. The weight contents of LSMO nanoparticles, PPy and oleic acid in case of the composite samples as determined by XPS are shown in Table 5.6. The last column shows the values of the saturation magnetization, the data was normalized to the content of LSMO specific for each sample.

Table 5.6. The weight contents of LSMO, PPy and oleic acid in case of the composite samples as determined by XPS. The last column shows the saturation magnetizations  $M_s$  normalized by the LSMO content

Sample	LSMO wt%	PPy wt%	oleic acid wt%	$M_s$ (emu/g <sub>LSMO</sub> )
LSMO	-	-	-	55.67
#1	82.8	14.3	2.9	68.21
#1'	84.0	16.0	-	65.53
#2	69.5	27.5	3	66.41
#2'	43.7	56.3	-	86.13
#3	47.7	39.8	12.5	68.10
#4	22.2	68.3	9.5	132.08

The magnetization curves at room temperature of the bare LSMO nanoparticles together with the LSMO / PPy nanocomposites are presented in Fig.5.29. As expected, the magnetization of different combinations of PPy and LSMO nanoparticles together with the bare LSMO nanoparticles covered or not with oleic acid as surfactant does not show any hysteresis loop, being consistent with a superparamagnetic behavior [82]. The temperature dependences of the magnetizations in ZFC-FC regimes for the LSMO nanoparticles and the LSMO@PPy composites are

shown in Fig. 5.30. As expected, a typical superparamagnetic behavior is evidenced in this figure.

As one can observe in Fig. 5.29 the saturation magnetizations  $M_S$  for the LSMO@PPy composites have larger values than the saturation magnetization of bare LSMO nanoparticles. The effect of PPy attached to the nanoparticles or the combined effect of both surfactants and PPy leads to an increase of the saturation magnetizations for all the nanocomposites samples as compared with the LSMO nanoparticles. The same type of increase of  $M_S$  has been recently reported for the oleic acid coating and PPy coating of magnetite nanoparticles respectively [67-69]. It seems that the attachment of organic molecules to the surface of magnetic nanoparticles could induce a reduction of the surface spin disorder resulting in an increase of the saturation magnetization values.

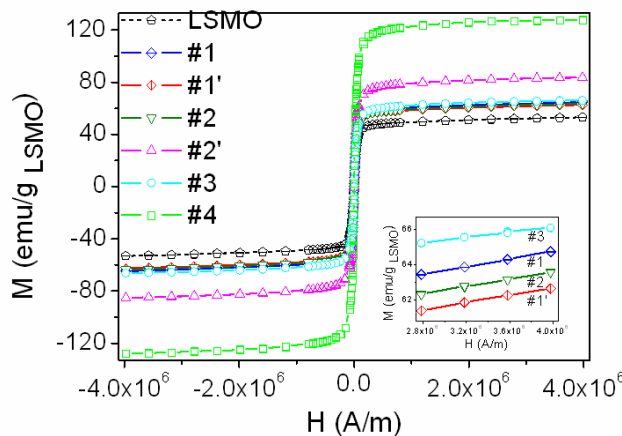


Fig. 5.29 The magnetization curves of the PPy nanocomposites as a function of the applied magnetic field, at room temperature. The absolute magnetizations are calculated referred to the LSMO content of each specific nanocomposite. Details are shown in the inset

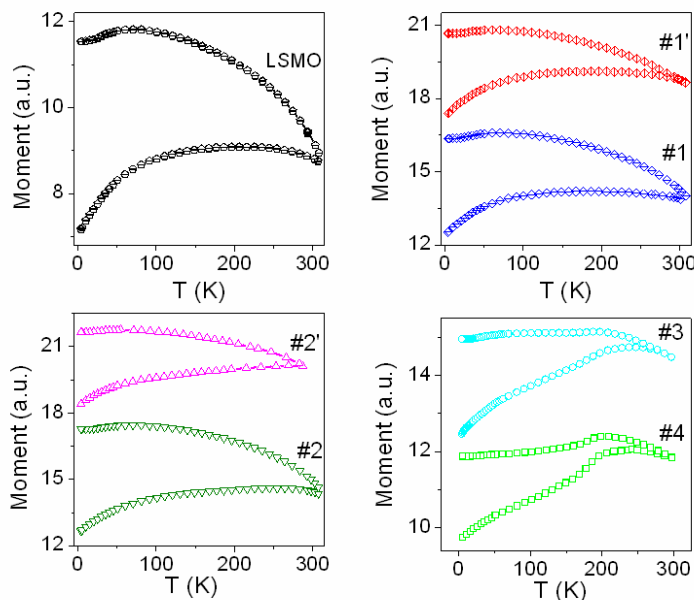


Fig. 5.30. Temperature dependence of the magnetization under ZFC-FC regimes for the magnetic nanocomposites samples and bare LSMO nanoparticles. The applied magnetic field was 1000e

To check if a charge transfer, going from PPy polymer to the LSMO nanoparticles, also occurs in our composites samples XANES measurements were done. The Mn-K and La-L<sub>III</sub> edges were investigated for one of the LSMO@PPy composite sample #2. As a reference the same lines were recorded for the bare LSMO nanoparticles. Fig. 5.31 presents results of XANES measurements near the Mn K-edge. The insert presents derivative spectra, performed in order to derive eventual chemical shifts of the absorption edge, defined as the inflection point of the XANES

(Teo et al. 1983). No noticeable chemical shift corresponding to the transition from  $1s$  to final states of  $p$  symmetry is observed between the LSMO and the LSMO@PPy. That means, the empty state DOS of  $p$  symmetry is not affected by the polymer adsorption. On the contrary, with polymer adsorption, a redshift of about  $1eV$  is observed for the inflection point of the pre-edge peak, which is usually attributed to quadrupole transitions from  $1s$  to  $3d$  states and dipole transitions from  $1s$  to  $3d$  final states hybridized with  $4p$  [113-115].

A noticeable the enhancement of the pre-edge peak with polymer adsorption is observed. The ratio between the two pre-edge peaks is  $1.32 \pm 0.05$  when comparing absolute intensities, or  $1.28 \pm 0.03$  when comparing areas. If an initial mixture of  $(0.67) Mn^{3+} + (0.33) Mn^{4+}$  is ascribed to the bare LSMO states, this yields an average  $3d$  vacancy number of 6.33 electrons for a Mn atom. The increase by the above specified factors implies a depopulation of Mn  $3d$  states such that the number of  $3d$  holes becomes about 8. A configuration  $4s_0 3d_2$ , which corresponds to  $Mn^{5+}$  can be ruled out. Therefore, there are two outlines that may be proposed:

(i) formation of supplementary  $Mn^{4+}$  with configuration  $3d_3$  (an increase of the pre-edge peak by a factor of  $7/6$  may be explained), together with serious modification of the transition matrix element which is induced by the orbital shrinking around absorbing Mn ions. This effect yields an increased superposition of the  $1s$  state and final state ( $3d4p$ ) orbitals;

(ii) formation of supplementary  $Mn^{4+}$ , but with electronic configuration  $4s_1 3d_2$ , i.e. transfer of one electron from Mn  $3d$  to Mn  $4s$  partial DOS upon polymer adsorption.

The first outline is more plausible, involving the increase of the  $Mn^{4+}$  content can be correlated with the magnetization increase via the enhancement of the double-exchange interactions between manganese positions at the surface of the PPy covered nanoparticles. Within this picture the delocalized  $\pi$  electron of the PPy chains goes to the oxygen vacancies existing at or near the surface of LSMO nanoparticles. Actually the oxygen deficiency at the nanoparticle surface breaks the double-exchange between Mn ions creating some spin disordered layers and reducing the magnetization. The transferred DOS at oxygen vacancies reestablishes the double exchange interactions within the occupied  $e_g$  band hence increasing the overall magnetization with some contributions from the surface disordered layers. This effect is sustained by the observed increase of white peak intensity in the La-L<sub>III</sub> XANES spectrum in case of the LSMO@PPy composite as compared to the LSMO nanoparticles. The effect is ascribed to an increase of the oxidation degree of the La ions determined by the PPy  $\pi$  electrons DOS existing at the oxygen vacancies.

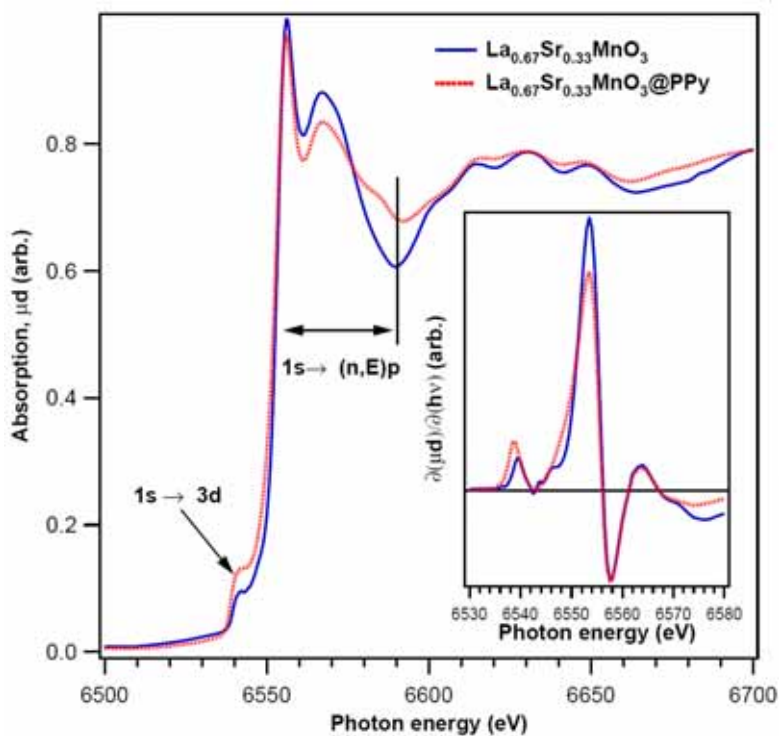


Fig. 5.31. Results of XANES measurements near the Mn K-edge. The insert presents the derivative spectra, performed in order to derive eventual chemical shifts of the absorption edge

## Chapter VI. Conclusions

### 6.1. Fe<sub>3</sub>O<sub>4</sub>@PPy nanocomposites

PPy-Fe<sub>3</sub>O<sub>4</sub> nanocomposites were obtained by the polymerization of Py in the presence of water based magnetic nanofluid. The surfactant nature (LA+DBS, MA+DBS, DBS+DBS) influences the size distribution of the magnetic nanoparticles in the nanofluid and ultimately the thickness of the PPy layer covering these nanoparticles in the nanocomposite.

The magnetization versus applied magnetic field of the reported nanocomposites does not show any hysteresis loop, which indicates a superparamagnetic behavior. FC and ZFC dependences of the magnetization versus temperature also evidence the superparamagnetic behavior of the nanocomposites. From the synthesis point of view the nature of the surfactants as well as the Py polymerization temperature are relevant synthesis parameters that allow tailoring the magnetic properties of the nanocomposites.

The surface modification of magnetite by PPy coating results in an increase in the saturation magnetization and of the apparent magnetic diameter of the nanoparticles due to a decrease in surface spin disorder. This novel effect is ascribed to a charge transfer process from the conducting polymer to the surface iron ions of magnetite. It involves the laterally delocalized  $\pi$  electrons of the conjugated PPy which could penetrate under the surface of magnetite nanoparticles.

The easy polymerization of PPy in stable dispersions of magnetic nanoparticles represents a good strategy to generate magnetic nanocomposites with controllable magnetic properties, which can be further easily provided with biofunctionality by the attachment of specific molecular groups to the polymer chains for applications in biotechnology.

### 6.2. Fe@Au nanocomposites

Core-shell Fe@Au nanoparticles were obtained by the inverse micelles method in different conditions.

In between the Fe(0) cores and the gold shells there is an additional shell of iron oxides as it results from the analysis of the Fe 2p core-level XPS lines.

Among the synthesis parameters, the molar ratio surfactant/HAuCl<sub>4</sub> influences strongly the nanoparticles size distribution and their magnetic properties. The narrowest size distribution was obtained for the Fe@Au sample prepared with the lowest value of surfactant/HAuCl<sub>4</sub> molar ratio while the highest magnetization resulted when the highest content of gold was put into the synthesis.

The size distribution of the nanoparticles influences strongly the magnetization values. For nanoparticles having greater mean magnetic (samples FA2

and FA3), due to the superparamagnetic blocking process, the saturation magnetization values are lower than for the nanoparticles with a thicker gold shell and a smaller magnetic diameter (FA1). This fact persists even if the particle size distribution and the corresponding energy barriers distributions (sample FA1 in Fig. 10) have multiple peaks.

The missing hysteresis loop in the magnetization *vs.* applied magnetic field represents a clear evidence for the superparamagnetic behavior for the core-shell Fe@Au nanoparticles. The superparamagnetic behavior is also evidenced from FC and ZFC dependences of the magnetization *vs.* temperature. The effective anisotropy constant,  $K_{\text{eff}}$  for the core-shell Fe@Au nanoparticles was obtained using the temperature dependence of the thermoremanent magnetization combined with magnetization *vs.* applied magnetic field.  $K_{\text{eff}}$  of core-shell Fe@Au nanoparticles increases linearly with the decrease of the iron core magnetic diameter  $D_0^{(m)}$ . The high value of surface contribution,  $K_S$  resulting from the linear dependence of  $K_{\text{eff}}$  *vs.*  $1/D_0^{(m)}$  is attributed to the combined shape and stress anisotropy at the gold–iron oxide–iron multiple interfaces.

### 6.3. La<sub>0.67</sub>Sr<sub>0.33</sub>MnO<sub>3</sub>@Au nanocomposites

Manganite nanoparticles La<sub>0.67</sub>Sr<sub>0.33</sub>MnO<sub>3</sub> having a mean diameter of 4.4nm were obtained by using the sol–gel procedure. By using the so-called seeding method, the LSMO nanoparticles were covered with gold forming core–shell like nanostructures.

Among the LSMO nanoparticles one can find few large particles (up to 50 nm) and as it appears from TEM images some clusters are formed. The surfactant layer on the manganite nanoparticle surfaces cannot avoid their aggregation due to the dipolar interactions.

The missing hysteresis loop in the magnetization *vs.* applied magnetic field represents a clear evidence for the superparamagnetic behavior for the LSMO@Au nanoparticles. Due to the magnetic dipole–dipole interactions the “magnetic” diameters of the nanoparticles appears to be at least twice larger than the real values as determined by TEM (here including both cores and shells). This assertion is sustained by the analysis of energy barrier distributions calculated from FC and ZFC temperature dependences of magnetizations. By going from LSA1 to the LSMO uncoated nanoparticles the mean number of interacting neighbors increases as the thickness of the Au shell decreases. As expected by gold coating the LSMO nanoparticles one can adjust the magnetic properties by reducing the strong magnetic dipole–dipole interactions between nanoparticles. By covering the LSMO cores with a properly adjusted gold shell one can diminish the tendency of the nanoparticles to form clusters and adjust the magnetic properties of the system.

The easy attachment to the nanoparticles gold surface of thiol containing molecules represents a good strategy to generate magnetic heterocomposites with controllable magnetic properties, which can be further easily provided with different

functionalities for applications as magnetic extraction, magnetic separation, biotechnologies, etc.

#### 6.4. $\text{La}_{0.67}\text{Sr}_{0.33}\text{MnO}_3$ @PPy nanocomposites

LSMO@PPy nanocomposites were obtained by the oxidative polymerization of pyrrole in presence of water dispersed LSMO nanoparticles. The polymerization produced some adhesive PPy layers around the magnetic nanoparticles leading thus to a core-shell structure evidenced by HRTEM.

The missing hysteresis loop in the magnetization vs. applied magnetic field represents a clear evidence for the superparamagnetic behavior for the core-shell Fe@Au nanoparticles. The superparamagnetic behavior is also evidenced from FC and ZFC dependences of the magnetization vs. temperature. A significant increase of the saturation magnetizations appears for all the samples when compared to the bare LSMO nanoparticles. The surface modification of manganite nanoparticles by polypyrrole coating results in a decrease of surface spin disorder. Therefore from the synthesis point of view the pyrrole polymerization is a relevant synthesis method that allows tailoring the magnetic properties of the LSMO nanocomposites.

Our results show for the first time that an enhancement of the magnetization could be obtained in the case of manganite nanoparticles coated with PPy due to the charge transfer from polymer  $\pi$  electronic states to some oxygen vacancies nearby the surface of the nanoparticles. This novel effect is ascribed to a charge transfer process from the conducting polymer to the surface iron ions of magnetite.

## Selected references

- [1] O. Pana, C. M. Teodorescu O. Chauvet, C. Payen, D. Macovei, R. Turcu, M.L. Soran, N. Aldea, Surf. Sci., 601, 4352(2007)
- [2] J. Chatterjee, Y. Haik, C. J. Chen, J. Magn. Mater. 246, 382(2002)
- [3] F. M. Mulder, R. C. Thiel, K. H. J. Buschow, J. Alloys Compd. 223, 127(1995)
- [4] L. Néel, Ann. Geophys. 99, 5(1949)
- [15] Jeffrey Pyun, Polymer Reviews, 47 (2007), 231
- [61] R.D. Sanchez, J. Rivas, M.A. Lopez-Quintela, M.T. Causa, M. Tovar, S.B. Oseroff, Appl. Phys. Lett. 68 (1) (1996)
- [62] J. Mahia, C. Vazquez-Vazquez, J. Mira, M.A. Lopez-Quintela, J. Rivas, T.E. Jones, S.B. Oseroff, J. Appl. Phys. 75 (10) (1994)
- [63] Y.H. Huang, Z.G. Xu, C.H. Yan, Z.M. Wang, T. Zhu, C.S. Liao, S. Gao, G.X. Xu, Solid State Commun. 114, 43-47 (2000)
- [64] Y.H. Huang, C.H. Yan, Z.M. Wang, C.S. Liao, G.H. Xu, Solid State Commun. 118, 541-546 (2001)
- [67] Turcu R, Pana O, Nan A, Craciunescu I, Chauvet O, Payen C (2008) J Phys D Appl Phys 41:245002.1– 245002.9
- [68] R. Turcu, A. Nan, O. Pana, I. Craciunescu, **C. Leostean**, I. Bratu, S. Macavei  
“Comparative study of smart composites based on magnetic nanoparticles and stimuli responsive polymers“ ECNP-2009-Paris
- [69] R. Turcu, A. Nan, I. Craciunescu, O. Pana, C. Falub, **C. Leostean**, S. Macavei, L. Vekas,  
”Functionalized polymer based magnetic nanostructures”, NANOTECH INSIGHT 2009, Barcelona
- [72] **C. Leostean**, O. Pana, R. Turcu, M. L. Soran, S. Macavei, O. Chauvet, C. Payen,  
“Comparative study of core–shell iron/iron oxide gold covered magnetic nanoparticles obtained in different conditions”  
J. Nanopart. Res., published 2011, on line first, DOI 10.1007/s11051-011-0313-3
- [73] Pana O, Turcu R, Soran ML, **Leostean C**, Gautron E, Payen C, Chauvet O (2010) Synth Met 160:1692–1698.
- [77] O Pana, N Gheorghe, ML Soran, **C Leostean**, S Macavei, E Gautron, CM Teodorescu, O Chauvet, “Interface charge transfer in polypyrrole coated perovskite manganite magnetic nanoparticles” NANO2010-Rome
- [82] Jacobs I S and Bean C P 1963 *Magnetism* vol 3, ed G T Rado and H Suhl (New York: Academic) p 271
- [83] Batle X and Labarta A 2002 *J. Phys. D: Appl. Phys.* 35 R15
- [84] Tronc E *et al* 1999 *J. Magn. Mater.* 200 552
- [85] Blanco-Mantecón M and O’Grady K 2006 *J. Magn. Mater.* 296 124
- [86] Guardia P, Batlle-Brugal B, Roca A G, Iglesias O, Morales M P, Serna C J, Labarta A and Batlle X 2007 *J. Magn. Mater.* 316 e756

- [87] Del Bianco L, Fiorani D, Testa A M, Bonetti E, Savini L and Signoretti S 2008 *Phys. Rev. B* 66 174418
- [88] Dormann J L, D’Orazio F, Lucari F, Tronc E, Prene P, Jolivet J P, Fiorani D, Cherkaoui R and Nogues M 1996 *Phys. Rev. B* 53 14291
- [89] Martinez B, Obradors X, Balcells L, Rouanet A and Monty C 1998 *Phys. Rev. Lett.* 80 181
- [90] Vargas J M, Socolovsky L M, Knobel M and Zanchet D 2005 *Nanotechnology* 16 S285–90
- [91] Goya G F, Berquo T S, Fonseca F C and Morales M P 2003 *J. Appl. Phys.* 94 3520
- [92] Chantrell R W, Popplewell J and Charles S W 1978 *IEEE Trans. Magn.* 14 975
- [93] Leslie-Pelecky D L and Rieke R D 1996 *Chem. Mater.* 8 1770
- [94] Rasa M 2000 *Eur. Phys. J. E* 2 265
- [95] Sappey R, Vincent E, Hadacek N, Chaput F, Boilot JP, Zins D (1997) *Phys Rev B* 56:14551–14559.
- [96] Néel L 1949 *C.R. Acad. Sci., Paris* 228 664
- [97] Street G B 1986 *Handbook of Conducting Polymers* vol 1, ed T A Skotheim (New York: Dekker) pp 279
- [98] Bentley F F, Smithson L D and Rozek A L 1968 *Infrared Spectra and Characteristic Frequencies 700–300 cm<sup>-1</sup>* (New York: Interscience/Wiley) p 1528
- [99] Zerbi G, Gussoni M and Castiglioni C 1991 *Conjugated Polymers* ed J L Bredas and R Silbey (Dordrecht: Kluwer) pp 435–507
- [100] Davidson R G and Turner T G 1995 *Synth. Met.* 72 121
- [101] Mills P, Sullivan JL (1983) *J Phys D Appl Phys* 16:723–732
- [102] Wang C, Baer DR, Amonette JE, Engelhard MH, Antony J, Qiang Y (2009) *J Am Chem Soc* 131:8824–8832
- [104] Gangopadhyay S, Hadjipanayis GC, Dale B, Sorensen CM, Klabunde KJ, Papaefthymiou V, Kostikas A (1992) *Phys Rev B* 45:9778–9787.
- [105] J. Mira, J. Rivas, F. Rivadulla, C. Vázquez-Vázquez, M.A. López-Quintela, *Phys. Rev. B*60(1999)2998.
- [106] M.P. Gutiérrez, J.H. Olivares, I. Betancourt, F. Morales, *J.Mater.Res.*24(2009) 1585.
- [108] M. El-Hilo, K. O’Grady, R.W. Chantrell, *J. Magn. Mater.*114(1992)295.
- [109] S. Shtrikman, E.P. Wohlfarth, *Phys. Lett. A* 85(1981)467.
- [110] J.L. Dormann, L. Bessasis, D. Fiorani, *J. Phys. C* 21(1988)2015.
- [113] Ghigna P, Carollo A, Flor G, Malavasi L, G Subias (2005) *J Phys Chem B* 109 4365-4372
- [114] Bridges F, Booth CH, Anderson M, Kwei GH, Neumeier JJ, Snyder J, Mitchell J, Gardner JS, Brosha E (2001) *Phys Rev B* 63 214405.
- [115] Subías G, García J, Proietti MG, Blasco J (1997) *Phys Rev B* 56 8183.

## List of published papers

- C. Leostean**, O. Pana, R. Turcu, M. L. Soran, S. Macavei, O. Chauvet, C. Payen,  
“*Comparative study of core–shell iron/iron oxide gold covered magnetic nanoparticles obtained in different conditions*”  
J. Nanopart. Res., published 2011, on line first, DOI 10.1007/s11051-011-0313-3
- O. Pana, R. Turcu, M.L. Soran, **C. Leostean**, E. Gautron, C. Payen, O. Chauvet,  
“*Synthesis and characterization of the core-shell Au covered LSMO manganite magnetic nanoparticles*”  
2010 Synthetic Metals 160 (15-16), pp. 1692-1698
- A. Nan, R. Turcu, I. Bratu, **C. Leostean**, O. Chauvet, E. Gautron, J. Liebscher,  
“*Novel magnetic core-shell Fe<sub>3</sub>O<sub>4</sub> polypyrrole nanoparticles functionalized by peptides or albumin*”  
2010 Arkivoc 2010 (10), pp. 185-198
- R. Turcu, A. Nan, I. Craciunescu, **C. Leostean**, S. Macavei, A. Taculescu, O. Marinica, C. Daia, L. Vekas,  
“*Synthesis and characterization of magnetically controllable nanostructures using different polymers*”  
2010 AIP Conference Proceedings 1311, pp. 20-27
- O. Pana, R. Turcu, M.L. Soran, S. Macavei, **C. Leostean**,  
“*Synthesis and characterization of LSMO nanoparticles covered with Au having a core-shell structure*”  
2009 Journal of Physics: Conference Series 182 (1), art. no. 012071
- R. Turcu, A. Nan, I. Craciunescu, O. Pana, **C. Leostean**, S. Macavei,  
“*Smart composites based on magnetic nanoparticles and responsive polymers*”  
2009 Journal of Physics: Conference Series 182 (1), art. no. 012081
- A. Nan, R. Turcu, I. Craciunescu, **C. Leostean**, I. Bratu, J. Liebscher,  
“*Surface initiated ring-opening polymerization of lactones on iron oxide nanoparticles*”  
2009 Journal of Physics: Conference Series 182 (1), art. no. 012070
- I. Craciunescu, A. Nan, R. Turcu, I. Kacso, I. Bratu, **C. Leostean**, L. Vekas,  
“*Synthesis, characterization and drug delivery application of the temperature responsive pNIPA hydrogel*”  
2009 Journal of Physics: Conference Series 182 (1), art. no. 012060
- C. Leostean**, O. Pana, R. Turcu, M. L. Soran  
“*Preperities of novel Fe@Au core-shell nanoparticles*”  
Studia Universitatis Babes-Bolyai, Physica, LIII,2 2008

## List of communications

O.Pana, O.Chauvet, C.Payen, E.Gautron, R.Turcu, C.M.Teodorescu, M.L.Soran, N.Aldea, **C.Leostean** "Synthesis and characterization of the core-shell magnetic nanostructures with noble metals", E-MRS 2007 Spring Meeting Strasbourg, France, 28 May-1 June, 2007

O.Pana, C.M.Teodorescu, O.Chauvet, C.Payen, R.Turcu, N.Aldea, M.L.Soran, **C.Leostean**, "Structure, morphology and magnetic properties of core-shell nanoparticles", Magnetic nanoparticles, composite materials and optical applications, St. Etienne, France, 3-9 Sept 2007

O. Pana, R. Turcu, M. L. Soran, **C. Leostean**, O. Chauvet, C. Payen, E. Gautron, "Functionalized core-shell magnetic nanostructures", E-MRS 2008 Spring Meeting Strasbourg (France), May 26- 30, 2008

M.L. Soran, O. Pana, A. Nan, **C. Leostean**, I. Bratu, "Synthesis and spectroscopic characterization of hybrid magnetic nanoparticles, based on Fe@Au and N-succinimide", Advanced Spectroscopies on Biomedical and Nanostructured Systems, 7-10 SEPT 2008, Cluj-Napoca, Romania

O. Pana, J. Martin, M. L. Soran, R. Turcu, **C. Leostean**, C. Mijangos, "Hybrid magnetic nanocomposites based on core – shell magnetic nanoparticles with polymers", 5th International Conference on NANOSTRUCTURED POLYMERS AND NANOCOMPOSITES, Paris – France, April 15-17, 2009

R. Turcu, A. Nan, O. Pana, I. Craciunescu, **C. Leostean**, I. Bratu, S. Macavei, "Comparative study of smart composites based on magnetic nanoparticles and stimuli responsive polymers", 5th International Conference on NANOSTRUCTURED POLYMERS AND NANOCOMPOSITES, Paris – France, April 15-17, 2009

O. Pana, R. Turcu, M.L. Soran, **C. Leostean**, O. Chauvet, C. Payen, "Hybrid nanocomposites based on gold covered core –shell functionalized magnetic nanoparticles", NANOTECH INSIGHT 29 March – 2 April 2009, Barcelona

R. Turcu, A. Nan, I. Craciunescu, O. Pana, C. Falub, **C. Leostean**, S. Macavei, L.Vekas, "Functionalized polymer based magnetic nanostructures", NANOTECH INSIGHT 29 March – 2 April 2009, Barcelona

A. Nan, R. Turcu, I. Craciunescu, **C. Leostean**, S. Macavei, H. Scharf, J. Liebscher, „New synthetic methods of magnetic core-shell nanoparticles by surface-initiated ring-opening polymerization of caprolactone", XX<sup>th</sup> International Symposium on Bioelectrochemistry and Bioenergetics, Sibiu, Romania, May 10-14, 2009.

A. Nan, R. Turcu, I. Craciunescu, **C. Leostean**, I. Bratu, J. Liebscher, "Surface initiated ring-opening polymerization of lactones on iron oxide nanoparticles", Processes in Isotopes and Molecules, 2009, september 24 – 26, Cluj-Napoca, Romania.

I. Craciunescu, A. Nan, R. Turcu, I. Kacso, I. Bratu, **C. Leostean**, L. Vekas, "Synthesis, characterization and drug delivery application of the temperature responsive pNIPA hydrogel", Processes in Isotopes and Molecules"2009, september 24 – 26, Cluj-Napoca, Romania

R. Turcu, A. Nan, I. Craciunescu, O. Pana, **C. Leostean**, S. Macavei, "Smart composites based on magnetic nanoparticles and responsive polymers", Processes in Isotopes and Molecules 2009, september 24 – 26, Cluj-Napoca, Romania.

R. Turcu, I. Craciunescu, A. Nan, O. Pana, **C. Leostean**, L. Vekas, A. Taculescu, "Encapsulation of functionalized magnetic nanoparticles in polymeric gels", 8<sup>th</sup> International Conference on Advanced Polymers via Macromolecular Engineering, Dresden, Germany, October 4-7, 2009.

R. Turcu, I. Craciunescu, A. Nan, O. Pana, **C. Leostean**, S. Macavei, D. Bica †, E. Gautron, O. Chauvet, "Biocompatible polymer coated magnetic nanoparticles systems", Workshop: Structural aspects of biocompatibleferrofluids: stabilization, properties control and application, GKSS Research Centre Geesthacht, Germany, 28-29 January 2010.

O. Pana, N.G. Gheorghe, **C. Leostean**, M.L. Soran, S. Macavei, R. Turcu, C.M. Teodorescu, "Polypyrrole coated magnetite and perovskite magnetic nanoparticles", Polymer-Nano-Particles Interaction: Concepts, Observations and Applications, 28-31 martie 2010, Physikzentrum Bad Honnef, Germania

A.Nan, R. Turcu, I. Craciunescu, **C. Leostean**, J. Liebscher, "Advanced method for Surface Ring-Opening Polymerization of Lactones on Magnetic Nanoparticles", "6th Conference on Nanostructured Polymers and Nanocomposites", Madrid, Spain, April 28-30, 2010

R. Turcu, A. Nan, I. Craciunescu, O. Pana, **C. Leostean**, S. Macavei, L. Barbu, "Design of magnetic nanostructures using different polymers or block copolymers for magnetic nanoparticles encapsulation", Nanotheranostics: Fabrication and Safety Concerns, Ayia Napa, Cyprus April 27<sup>th</sup> - April 30<sup>th</sup>, 2010

R. Turcu, A. Nan, I. Craciunescu, **C. Leostean**, S. Macavei, A. Taculescu, O. Marinica, L. Vekas, "Synthesis And Characterization Of Biocompatible Magnetically Controllable Nanostructures Using Different Polymers", 8<sup>th</sup> International Conference on the Scientific and Clinical Applications of Magnetic Carriers - Rostock, Germany, May 25-29, 2010

A. Nan, R. Turcu, I. Craciunescu, I. Bratu, **C. Leostean**, S. Karsten, S. Källäne, L. Vekas, J. Liebscher, "Application of click chemistry for functionalization of polypyrrole coating the magnetic nanoparticles", 8<sup>th</sup> International Conference on the Scientific and Clinical Applications of Magnetic Carriers - Rostock, Germany, May 25-29, 2010

O. Pana, N.G. Gheorghe, **C. Leostean**, M.L. Soran, R. Turcu, C.M. Teodorecu, "Magnetization enhancement by polypyrrole coating of magnetic nanoparticles", 11th International Balkan Workshop on Applied Physics, 2010, Iulie, Constanta

I. Craciunescu, A. Nan, R. Turcu, I. Bratu, **C. Leostean**, L. Vekas, "Synthesis And Characterisation Of Dual Sensitive Magnetic Microgels", 11th International Balkan Workshop on Applied Physics, 2010, 7-9 iulie, Constanta

O. Pana, N.G. Gheorghe, M. L. Soran, **C. Leostean**, S. Macavei, E. Gautron, C.M. Teodorescu, O. Chauvet, "Interface charge transfer polypyrrole coated perovskite manganite magnetic nanoparticles", International conference on nanostructured materials - NANO 2010, Rome, sept. 13 – 17, 2010

**C. Leostean**, O. Pana, R. Turcu, M. L. Soran, S. Macavei, O. Chauvet, C. Payen, "Comparative study of core-shell iron/iron oxide gold covered magnetic nanoparticles obtained in different conditions", International conference on nanostructured materials - NANO 2010, Rome, sept. 13 – 17, 2010

R. Turcu, A. Nan, I. Craciunescu, **C. Leostean**, C. Podaru, L. Vekas, E. Gautron, O. Chauvet, "Biofunctionalization of Magnetic Nanoparticles by Polymer and Copolymer Coating", 5<sup>th</sup> International Conference on Surfaces, Coatings and Nano-Structured Materials, NANOSMAT-5, Reims, France, 19-21 October 2010

O. Pana, N.G. Gheorghe, **C. Leostean**, M.L. Soran, S. Macavei, C.M. Teodorescu, "Polypyrrole coated core-shell magnetic nanoparticles: magnetization enhancement and interface charge transfer studied by XANES", Second Conference on Multifunctional, Hybrid and Nanomaterials, 6-10 martie Strasbourg, Franta

O. Pana, N.G. Gheorghe, **C. Leostean**, M.L. Soran, S. Macavei, N. Aldea, C.M. Teodorescu, "Interface charge transfer of polypyrrole coated manganite nanoparticles and magnetization enhancement studied by XANES and EXAFS", E-MRS 2011 SPRING MEETING - IUMRS ICAM 2011 & E-MRS / MRS BILATERAL CONFERENCE on ENERGY, 9-13 mai, Nice, Franta

A. Nan, R. Turcu, I. Craciunescu, I. Bratu, **C. Leostean**, S. Karsten, L. Vekas, J. Liebscher, "Functionalized core-shell nanostructures based on conducting polypyrrole coating magnetic nanoparticles", Workshop „Multifunctional nanoparticles, magnetically controllable fluids, complex flows and applications”, 2-3 June, 2011 Timisoara, Romania

M.L. Soran, O. Pana, **C. Leostean**, M. Stefan, C. Bele, C. Matea, "Single -Walled Carbon Nanotubes Functionalized by Fe@Au Nanoparticles", 5th INTERNATIONAL MEETING ON DEVELOPMENTS IN MATERIALS, PROCESSES AND APPLICATIONS OF EMERGING, 27-29 iunie 2011, Portugalia

O. Pana, M.L. Soran, **C. Leostean**, M. Stefan, S. Macavei, "Platinum Based Magnetic Nanoparticles and Functionalized Composites", 5th INTERNATIONAL MEETING ON DEVELOPMENTS IN MATERIALS, PROCESSES AND APPLICATIONS OF EMERGING, 27-29 iunie 2011, Portugalia